

UNIVERSITÉ DU QUÉBEC À MONTRÉAL

LA VARIABILITÉ INTER- ET INTRA-SAISONNIÈRE DU COUPLAGE
TERRE-ATMOSPHÈRE EN AMÉRIQUE DU NORD DANS LA CINQUIÈME
GÉNÉRATION DU MODÈLE RÉGIONAL CANADIEN DU CLIMAT (MRCC5)

MÉMOIRE
PRÉSENTÉ
COMME EXIGENCE PARTIELLE
DE LA MAÎTRISE EN SCIENCES DE L'ATMOSPHÈRE

PAR
GREGORY YANG KAM WING

JUIN 2016

UNIVERSITÉ DU QUÉBEC À MONTRÉAL
Service des bibliothèques

Avertissement

La diffusion de ce mémoire se fait dans le respect des droits de son auteur, qui a signé le formulaire *Autorisation de reproduire et de diffuser un travail de recherche de cycles supérieurs* (SDU-522 – Rév.07-2011). Cette autorisation stipule que «conformément à l'article 11 du Règlement no 8 des études de cycles supérieurs, [l'auteur] concède à l'Université du Québec à Montréal une licence non exclusive d'utilisation et de publication de la totalité ou d'une partie importante de [son] travail de recherche pour des fins pédagogiques et non commerciales. Plus précisément, [l'auteur] autorise l'Université du Québec à Montréal à reproduire, diffuser, prêter, distribuer ou vendre des copies de [son] travail de recherche à des fins non commerciales sur quelque support que ce soit, y compris l'Internet. Cette licence et cette autorisation n'entraînent pas une renonciation de [la] part [de l'auteur] à [ses] droits moraux ni à [ses] droits de propriété intellectuelle. Sauf entente contraire, [l'auteur] conserve la liberté de diffuser et de commercialiser ou non ce travail dont [il] possède un exemplaire.»

REMERCIEMENTS

Avant de commencer la présentation de ce mémoire, je tiens à exprimer mes sincères remerciements à toutes les personnes qui y ont contribué. Tout d'abord, je voudrais remercier la professeure Laxmi Sushama de m'avoir guidé tout au long du projet, et poussé à dépasser mes limites afin de réaliser de la recherche de qualité. Je suis également infiniment reconnaissant envers mon collaborateur, Gulilat Tefera Diro, de m'avoir initié à la recherche scientifique, et aidé dans le développement de ce mémoire.

Je remercie Bruno Fang, Arlette Chacón, Dae Il Jeong et Katja Winger de m'avoir aidé à régler les nombreux problèmes que j'ai rencontrés pendant ces deux années intensives.

Je voudrais aussi exprimer ma gratitude envers le centre ESCER de m'avoir donné l'opportunité de faire mes preuves en tant qu'étudiant à la maîtrise, ainsi que tous les professeurs, qui m'ont transmis des connaissances qui me seront utiles tout au long de ma vie.

Je souhaite aussi remercier Étienne, Ismat et Karen de m'avoir soutenu dans l'écriture de ce manuscrit et la préparation des présentations orales, et ma mère, Shirley, et ma soeur, Catherine, pour leur soutien moral. Enfin, je dédie ce mémoire à mon père, Philip, qui nous a quittés il y a un an.

TABLE DES MATIÈRES

LISTE DES FIGURES	vii
LISTE DES TABLEAUX	xi
LISTE DES ACRONYMES	xiii
LISTE DES SYMBOLES	xvii
RÉSUMÉ	xix
CHAPITRE I	
INTRODUCTION	1
1.1 Problématique et objectifs du mémoire	1
1.2 Méthodologie	5
1.3 Organisation du mémoire	8
CHAPITRE II	
THE INTER- AND INTRA-SEASONAL VARIABILITY OF LAND-ATMOSPHERE COUPLING OVER NORTH AMERICA IN THE FIFTH GENERATION CA- NADIAN REGIONAL CLIMATE MODEL (CRCM5)	9
Abstract	10
2.1 Introduction	11
2.2 Model, methods and observational data	14
2.2.1 Model	14
2.2.2 Methods and observational data	15
2.3 Soil moisture-temperature coupling in current climate	18
2.3.1 Model evaluation	18
2.3.2 Coupling strength and underlying mechanisms	19
2.3.3 Influence of soil moisture variability on temperature extremes	21
2.4 Projected changes to soil moisture-temperature coupling	23
2.4.1 Coupling strength and underlying mechanisms	23

2.4.2 Influence of soil moisture variability on temperature extremes . . .	27
2.5 Summary and conclusions	28
Figures	33
Tables	47
CHAPITRE III	
CONCLUSION	49
ANNEXE A	
FIGURES COMPLÉMENTAIRES	55
RÉFÉRENCES	59

LISTE DES FIGURES

Figure	Page
2.1 (a) Observed (CRU) mean seasonal two-meter temperatures and (b) their interannual variability ($^{\circ}\text{C}$) (top panels) and differences between the CRCM5 simulation driven by ERA Reanalyses and CRU ($\text{CRCM5} - \text{ERA}_{\text{coupled}} - \text{CRU}$) (bottom panels).	34
2.2 (a) Observed (CMC) mean seasonal snow depths and (b) their interannual variability (cm) (top panels) and differences between the CRCM5 simulation driven by ERA Reanalyses and CMC ($\text{CRCM5} - \text{ERA}_{\text{coupled}} - \text{CMC}$) (bottom panels).	35
2.3 (a) Observed (ISCCP) mean seasonal surface albedos and (b) their interannual variability (%) (top panels) and differences between the CRCM5 simulation driven by ERA Reanalyses and ISCCP ($\text{CRCM5} - \text{ERA}_{\text{coupled}} - \text{ISCCP}$) (bottom panels).	36
2.4 (a) Soil moisture-temperature coupling strength ($^{\circ}\text{C}$) ($\Delta\sigma = \sigma_{T,\text{coupled}} - \sigma_{T,\text{uncoupled}}$) over North America from the ERA-driven CRCM5 simulation for the 1981–2010 period ($\text{CRCM5} - \text{ERA}$) for the March to December period, and (b) zonally averaged monthly soil moisture-temperature coupling strength from $\text{CRCM5} - \text{ERA}$, for the region enclosed by 115°W – 95°W and 48°N – 58°N shown in the middle top panel.	37
2.5 (a) Interannual variability of the fraction of soil liquid water for the coupled ERA-driven CRCM5 simulation ($\text{CRCM5} - \text{ERA}_{\text{coupled}}$), and differences in interannual variability between coupled and uncoupled ERA-driven CRCM5 simulations ($\text{CRCM5} - \text{ERA}$) ($\Delta\sigma = \sigma_{\text{coupled}} - \sigma_{\text{uncoupled}}$) averaged over 115°W – 95°W for (b) snow depth (cm), (c) surface albedo (%), (d) cloud cover (%), (e) net shortwave radiation (W/m^2), (f) soil temperature ($^{\circ}\text{C}$), (g) upwelling longwave radiation (W/m^2), and (h) latent heat flux (W/m^2).	38

2.6	(a) 90th percentile of daily maximum temperature ($^{\circ}\text{C}$) from observations, (b) differences between the 90th percentile of maximum temperature ($^{\circ}\text{C}$) from coupled CRCM5 simulations ($\text{CRCM5} - \text{ERA}_{\text{coupled}}$) and that from observations, and (c) differences in the mean number of hot days between coupled and uncoupled ERA-driven CRCM5 simulations ($\text{CRCM5} - \text{ERA}_{\text{coupled}} - \text{CRCM5} - \text{ERA}_{\text{uncoupled}}$) for the 1981–2010 period.	39
2.7	As in Figure 2.4, but for the CanESM2-driven CRCM5 simulation performed for the 1981–2010 period ($\text{CRCM5} - \text{CanC}$).	40
2.8	Differences in interannual variability between coupled and uncoupled simulations ($\Delta\sigma = \sigma_{\text{coupled}} - \sigma_{\text{uncoupled}}$) for (a) snow depth (cm), (b) cloud cover (%) and (c) net shortwave radiation (W/m^2) for CanESM2-driven CRCM5 simulations ($\text{CRCM5} - \text{CanC}$) (left), and the comparison between CanESM2-driven and ERA-driven CRCM5 simulations ($\text{CRCM5} - \text{CanC} - \text{CRCM5} - \text{ERA}$) (right).	41
2.9	As in Figure 2.4, but for the CanESM2-driven CRCM5 simulation performed for the 2071–2100 period for the RCP 4.5 scenario ($\text{CRCM5} - \text{CanRCP4.5}$).	42
2.10	As in Figure 2.4, but for the CanESM2-driven CRCM5 simulation performed for the 2071–2100 period for the RCP 8.5 scenario ($\text{CRCM5} - \text{CanRCP8.5}$).	43
2.11	Differences in interannual variability between coupled and uncoupled CanESM2-driven CRCM5 simulations ($\Delta\sigma = \sigma_{\text{coupled}} - \sigma_{\text{uncoupled}}$) for the 2071–2100 period for RCPs 4.5 (left) and 8.5 (right) for (a) snow depth (cm), (b) surface albedo (%), and (c) downwelling longwave radiation (W/m^2).	44
2.12	(a) Differences between the 90th percentile of maximum temperature ($^{\circ}\text{C}$) obtained from CanESM2-driven CRCM5 simulations ($\text{CRCM5} - \text{CanC}$) and that from observations, and (b) differences in the mean number of hot days between coupled and uncoupled CanESM2-driven CRCM5 simulations ($\text{CRCM5} - \text{CanC}_{\text{coupled}} - \text{CRCM5} - \text{CanC}_{\text{uncoupled}}$) for the 1981–2010 period.	45

2.13	Differences in the mean number of hot days between coupled and uncoupled CanESM2-driven CRCM5 simulations for the 2071–2100 period for the (a) RCP 4.5 ($\text{CRCM5} - \text{CanRCP4.5}_{\text{coupled}} - \text{CRCM5} - \text{CanRCP4.5}_{\text{uncoupled}}$) and (b) RCP 8.5 ($\text{CRCM5} - \text{CanRCP8.5}_{\text{coupled}} - \text{CRCM5} - \text{CanRCP8.5}_{\text{uncoupled}}$) scenarios.	46
------	---	----

LISTE DES TABLEAUX

Tableau	Page
2.1 List of experiments considered in this study	48

LISTE DES ACRONYMES

MRCs	Modèles régionaux du climat
MGCs	Modèles globaux du climat
MRCC5/CRCM5	Cinquième génération du modèle régional canadien du climat / Fifth generation Canadian Regional Climate Model
ERA	European Centre for Medium-Range Weather Forecasts Re-Analysis
CanESM2	Second generation Canadian Earth System Model
GLACE	Global Land Atmosphere Coupling Experiment
GCMs	Global Climate Models
RCMs	Regional Climate Models
CHRM	Climate High-Resolution Model
ICTP RegCM	International Center for Theoretical Physics Regional Climate Model
WRF	Weather Research and Forecasting
NCAR CLM	National Center for Atmospheric Research Community Land Model
GEM	Global Environment Multiscale
CLASS	Canadian Land Surface Scheme

RCP	Representative Concentration Pathway
IPCC	Intergovernmental Panel on Climate Change
AR5	Fifth Assessment Report
CRU	Climate Research Unit
ISCCP	International Satellite Cloud Climatology Project
NASA	National Aeronautics and Space Administration
CMC	Centre Météorologique Canadien / Canadian Meteorological Center
MAM	March, April, May
DJF	December, January, February
CRCM5 – ERA _{coupled}	Simulation with interactive soil moisture driven by ERA-40 / ERA-Interim Reanalysis for the 1981–2010 period
CRCM5 – ERA _{uncoupled}	Simulation with prescribed soil moisture driven by ERA-40 / ERA-Interim Reanalysis for the 1981–2010 period
CRCM5 – CanC _{coupled}	Simulation with interactive soil moisture driven by CanESM2 for the 1981–2010 period
CRCM5 – CanC _{uncoupled}	Simulation with prescribed soil moisture driven by CanESM2 for the 1981–2010 period
CRCM5 – CanRCP4.5 _{coupled}	Simulation with interactive soil moisture driven by CanESM2 (RCP 4.5) for the 2071–2100 period
CRCM5 – CanRCP4.5 _{uncoupled}	Simulation with prescribed soil moisture driven by CanESM2 (RCP 4.5) for the 2071–2100 period
CRCM5 – CanRCP8.5 _{coupled}	Simulation with interactive soil moisture driven by CanESM2 (RCP 8.5) for the 2071–2100 period
CRCM5 – CanRCP8.5 _{uncoupled}	Simulation with prescribed soil moisture driven by CanESM2 (RCP 4.5) for the 2071–2100 period

CNRCWP	Canadian Network for Regional Climate and Weather Processes
NSERC	Natural Sciences and Engineering Research Council
ECMWF	European Centre for Medium-Range Weather Forecasts
CMIP5	Coupled Model Intercomparison Project

LISTE DES SYMBOLES

$\sigma_{T,couplée} / \sigma_{T,coupled}$	Variabilité interannuelle de la température à deux mètres d'altitude dans la simulation couplée
$\sigma_{T,non-couplée} / \sigma_{T,uncoupled}$	Variabilité interannuelle de la température à deux mètres d'altitude dans la simulation non-couplée
$\sigma_{couplée} / \sigma_{coupled}$	Variabilité interannuelle d'une variable de surface ou atmosphérique dans la simulation couplée
$\sigma_{non-couplée} / \sigma_{uncoupled}$	Variabilité interannuelle d'une variable de surface ou atmosphérique dans la simulation non-couplée

RÉSUMÉ

Cette étude explore la variabilité inter- et intra-saisonnière du couplage entre l'humidité du sol et la température de l'air pour les régions des latitudes moyennes et élevées d'Amérique du Nord. À cet égard, des simulations couplées et non-couplées sont réalisées avec la cinquième génération du modèle régional canadien du climat (MRCC5). Dans les simulations couplées, la terre et l'atmosphère interagissent librement ; dans les simulations non-couplées, la variabilité interannuelle de l'humidité du sol est éliminée en remplaçant les contenus en eau liquide et solide par des moyennes climatologiques. Cette étude se penche également sur les projections futures du couplage en comparant des simulations couplées et non-couplées pour le climat actuel (1981–2010) et futur (2071–2100).

Les résultats pour le climat actuel indiquent que le couplage est important sur la région qui s'étend du sud des Grandes Plaines des États-Unis jusqu'au sud des Prairies canadiennes. Alors que le couplage sur les Grandes Plaines persiste à l'année longue, le couplage sur les Prairies suit l'évolution saisonnière du point de congélation. L'analyse du couplage sur les Prairies au printemps et en automne révèle un mécanisme différent de celui de l'été, la saison la mieux étudiée dans ce contexte. L'état de l'eau (liquide ou solide) dans le sol ainsi que la profondeur de la neige influencent l'albédo de surface, qui affecte le rayonnement court entrant et le rayonnement long sortant, et subséquemment la température de l'air. Pour les régions à fort couplage, les simulations couplées sont représentatives des températures extrêmes observées, et indiquent un nombre supérieur de journées chaudes comparées aux simulations non-couplées. Ceci suggère que la variabilité de l'humidité du sol peut amplifier la fréquence des températures extrêmes. Dans les projections futures, les changements dans le couplage varient selon les saisons : les sols plus secs renforcent le couplage en été, alors que des changements dans la profondeur de la neige et la couverture nuageuse influencent le couplage au printemps et en automne.

Mots-clés : humidité du sol, couplage terre-atmosphère, Amérique du Nord, modèle régional du climat, changement climatique, températures extrêmes

CHAPITRE I

INTRODUCTION

1.1 Problématique et objectifs du mémoire

Les anomalies dans les caractéristiques de la surface terrestre peuvent influencer l'atmosphère de diverses façons. L'humidité du sol, qui peut être définie comme étant le volume d'eau liquide dans un volume de sol donné [Seneviratne *et al.*, 2010], a fait l'objet de plusieurs études pour son influence sur la température de l'air et la précipitation [Seneviratne *et al.*, 2006 ; Koster *et al.*, 2006 ; Tawfik et Steiner, 2011 ; Diro *et al.*, 2014]. En perturbant le bilan d'énergie à la surface, la variabilité de l'humidité du sol peut influencer la variabilité de la température de l'air et celle de la précipitation. En été, l'humidité du sol influence surtout l'évapotranspiration. Ceci influence la répartition du rayonnement net dans les flux de chaleur latente et sensible, qui affectent la température de l'air [Pal et Eltahir, 2001]. De plus, l'influence de l'humidité du sol sur l'évapotranspiration peut affecter la formation des nuages et au final la précipitation mais cette relation demeure difficile à décrire [Seneviratne *et al.*, 2010]. Pour des raisons de simplicité, ce mémoire sera donc surtout consacré à la relation entre l'humidité du sol et la température, communément appelé « le couplage entre l'humidité du sol et la température ». Plusieurs études ont démontré que les anomalies dans l'humidité du sol peuvent parfois être assez conséquentes pour mener à l'amplification et

la prolongation de phénomènes météorologiques extrêmes dévastateurs tels que les sécheresses, les inondations, et les vagues de chaleur. Par exemple, *Oglesby et Erickson* [1989] ont démontré l'importance de l'humidité du sol dans le prolongement et l'amplification de la sécheresse et de la chaleur extrême qui ont sévi aux Etats-Unis en 1988. Par ailleurs, *Fischer et al.* [2007a,b] ont démontré que les vagues de chaleur, qui ont affecté l'Europe en 1976, 1994, 2003, et 2005, ont été amplifiées par des conditions d'humidité du sol plus sèches que la normale. Ces résultats démontrent l'importance de l'humidité du sol dans la prévision des phénomènes météorologiques extrêmes. En effet, *Koster et al.* [2010] ont démontré que la capacité des modèles de prévision à prédire ce genre de phénomènes pourrait être améliorée à l'aide d'une meilleure initialisation des anomalies dans l'humidité du sol. Toutefois, l'importance de ces anomalies devrait être démontrée d'avantage. Alors, il est important d'approfondir nos connaissances sur les mécanismes du couplage entre l'humidité du sol et la température de l'air. Cependant, les données d'observations pour l'humidité du sol sont très éparses voir quasiment inexistantes pour certaines régions de l'Amérique du Nord. Il existe des analyses de surface et des données satellitaires pour l'humidité du sol, mais celles-ci couvrent principalement les États-Unis et non le Canada. Comme les processus du couplage ne peuvent également pas être observés aisément, la plupart des études sur le couplage sont réalisées à l'aide de modèles du climat.

Les modèles du climat donnent souvent des résultats divergents car ils utilisent des paramétrages physiques et des schémas de surface différents, et possèdent des conditions aux frontières latérales distinctes. Effectuer des expériences avec des modèles du climat n'est donc pas une méthode systématiquement fiable pour étudier le couplage. Comme les processus physiques peuvent être paramétrés de différentes façons, l'humidité du sol peut, par exemple, influencer la température de l'air avec une intensité qui varie énormément d'un modèle à un autre. Par exemple, dans le Global Land-Atmosphere Coupling Experiment (GLACE), *Koster et al.* [2006] ont observé que l'intensité du cou-

plage variait beaucoup parmi les 12 modèles globaux du climat (MGCs) participants. Par contre, les 12 modèles indiquaient tous que le couplage était particulièrement fort sur les zones semi-arides où le sol est particulièrement sec et donc grandement affecté par la variabilité de son contenu en eau liquide. Ainsi, dans ces régions, les changements dans l'humidité du sol peuvent jouer un rôle important dans les échanges d'énergie entre la surface terrestre et l'atmosphère. Cependant, il arrive que les MGCs aient également du mal à identifier toutes les régions à fort couplage dû à leur faible résolution. On utilise alors des modèles régionaux du climat (MRCs) pour étudier le couplage car ils permettent de réaliser des simulations avec une meilleure résolution.

Dans l'étude GLACE, les Grandes Plaines en Amérique du Nord ont été identifiées comme étant une région semi-aride où le couplage est particulièrement fort en été. Cette région a donc été beaucoup étudiée à travers des expériences réalisées avec des MRCs. Par exemple, *Diro et al.* [2014] ont observé que le couplage était en effet conséquent sur les Grandes Plaines dans la cinquième génération du modèle régional canadien du climat (MRCC5). Dans cette étude, ils ont également observé que la variabilité de l'humidité du sol avait un grand impact sur la fréquence et la durée des phénomènes météorologiques extrêmes en été. Avec le MRC, Regional Climate Model version 4.0 (RegCM 4.0), développé par le International Center for Theoretical Physics (ICTP) [*Giorgi et al.*, 2012], *Mei et al.* [2013] ont aussi observé un fort couplage sur le centre des États-Unis. Cependant, *Zhang et al.* [2008] ont obtenu un résultat légèrement différent avec la deuxième version du MRC, Weather Research and Forecasting (WRF) [*Skamarock et al.*, 2005] : le fort couplage qu'ils ont observé sur les États-Unis s'étendait sur une plus large région comparée aux autres études. Cette région couvrait non seulement les Grandes Plaines mais aussi le sud-ouest et le sud-est du continent Nord-Américain. De plus, en utilisant le Climate High-Resolution Model (CHRM) [*Vidale et al.*, 2003], *Seneviratne et al.* [2006] ont observé que le couplage était fort sur la région Méditerranéenne en Europe, une région semi-aride où le couplage était inexplicablement faible dans l'étude GLACE.

Ces différences suggèrent donc qu'il est important d'effectuer des études de comparaison de modèles pour mieux comprendre le couplage sous toutes ses formes.

Alors que le couplage en été a beaucoup été étudié, le couplage pendant les autres saisons a rarement été étudié car il est considéré comme étant trop faible pour avoir un réel impact sur le climat. Cependant, il ne faut pas ignorer les autres saisons car certaines études récentes ont démontré que le couplage pouvait en effet être fort à l'année longue. En fait, *Tawfik et Steiner* [2011] ont observé que le couplage était fort sur les Grandes Plaines pendant les saisons froides dans le Regional Climate Model (RegCM), un MRC couplé avec le schéma de surface, Community Land Model version 3.5 (CLM), et développé par le ICTP [*Pal et al.*, 2007 ; *Oleson et al.*, 2008]. Ils ont aussi démontré que l'état de l'eau dans le sol (les quantités d'eau liquide et de glace présentes) et son influence sur les flux de chaleur sortants jouaient un rôle plus important dans le couplage pendant ces saisons.

Tandis que les études mentionnées ci-haut se sont concentrées sur le climat actuel, d'autres ont aussi analysé les changements dans le couplage en été sous l'effet du réchauffement climatique. Dans leur étude sur le continent européen, *Seneviratne et al.* [2006] ont démontré que les régions à fort couplage pourraient se déplacer de la région méditerranéenne à l'Europe central dans le futur. Des résultats similaires ont été obtenus dans une étude effectuée sur l'Amérique du Nord par *Diro et Sushama* [2016]. Dans ces deux études, l'apparition d'un fort couplage dans des régions qui se situent plus au nord est probablement causée par des conditions du sol plus sèches, qui amplifient la dépendance de l'évapotranspiration sur l'humidité du sol. Néanmoins, ces résultats fournissent des informations sur les changements futurs du couplage uniquement pour l'été mais pas pour les autres saisons.

L'objectif de ce mémoire est donc d'utiliser la cinquième génération du modèle régional canadien du climat (MRCC5) afin de résoudre quatre problèmes :

1. Comment l'intensité du couplage évolue-t-elle de saison en saison ?
2. Quelles sont les différences saisonnières dans les mécanismes du couplage ?
3. Quel est l'effet des anomalies dans l'humidité du sol sur les températures extrêmes ?
4. Comment l'intensité et les mécanismes du couplage changeront-ils dans un climat futur plus chaud ?

Les résultats de cette étude nous permettront non seulement d'approfondir nos connaissances sur les mécanismes du couplage mais nous aideront également à démontrer qu'il est important d'améliorer la représentation des processus physiques contribuant au couplage dans les modèles du climat.

1.2 Méthodologie

Le MRC utilisé dans ce mémoire est la cinquième génération du modèle régional canadien du climat (MRCC5) [Zadra *et al.*, 2008], qui est adapté du modèle Global Environment Multiscale (GEM) [Côté *et al.*, 1998]. MRCC5 utilise le schéma de surface canadien (CLASS v3.5) [Verseghy, 1991 ; Verseghy *et al.*, 1993 ; Verseghy, 2011] qui fournit une représentation explicite de la végétation et de différents types de surface. Une configuration profonde du sol, qui comporte 26 niveaux pour une profondeur de 60 mètres, est utilisée.

Les simulations sont réalisées avec MRCC5 avec une résolution spatiale de $0,44^\circ$, ce qui équivaut à environ 50 km, et un pas de temps de 20 minutes. Le domaine d'étude comporte 212×200 points de grille au total. Les 20 points de grilles extérieurs servent de zone éponge et de zone de pilotage, et les 172×160 points de grilles intérieurs recouvrent l'Amérique du Nord dans son entièreté.

L'abilité du modèle à reproduire la distribution spatiale des moyennes saisonnières et de la variabilité interannuelle de la température de l'air, la profondeur de la neige, et l'albédo de surface est tout d'abord évaluée à l'aide de données d'observations obtenues de différentes sources. Des données de stations météorologiques, provenant du Climate Research Unit (CRU TS 3.1) [Harris *et al.*, 2014] sont considérées pour la température de l'air, des données satellitaires du International Satellite Cloud Climatology Project (ISCCP) [Rossow *et Schiffer*, 1999] sont obtenues pour calculer l'albédo de surface observé, et des données de stations météorologiques du Centre Météorologique Canadien (CMC) [Brown *et al.*, 2003] sont utilisées pour valider la profondeur de la neige.

L'intensité du couplage entre l'humidité du sol et la température de l'air est analysée en utilisant des simulations couplées et non-couplées réalisées avec MRCC5. Les simulations couplées sont réalisées avec MRCC5, piloté par les réanalyses ERA-40 [Uppala *et al.*, 2005] entre 1958 et 1978 et les réanalyses ERA-Interim [Dee *et al.*, 2011] entre 1979 et 2010. Une période de 30 ans allant de 1981 à 2010 est sélectionnée pour étudier le couplage dans le climat présent. Les simulations non-couplées possèdent les mêmes conditions aux frontières latérales que les simulations couplées. La seule différence entre les deux types de simulations réside dans le remplacement des contenus en eau liquide et en glace par des moyennes climatologiques à chaque pas de temps. Vu que cette modification isole la variabilité interannuelle de l'humidité du sol, la différence entre les simulations couplées et non-couplées nous permet de déterminer à quel point la variabilité de l'humidité du sol peut influencer diverses variables de surface et atmosphériques.

L'intensité du couplage entre l'humidité du sol et la température de l'air est tout simplement définie comme étant la différence de variabilité interannuelle dans la température de l'air à deux mètres d'altitude comme suit :

$$\Delta\sigma_T = \sigma_{T,couplée} - \sigma_{T,non-couplée} \quad (1.1)$$

où $\sigma_{T,couplée}$ et $\sigma_{T,non-couplée}$ représentent la variabilité interannuelle de la température à deux mètres pour la simulation couplée et non-couplée respectivement.

De la même façon, les mécanismes du couplage sont déterminés en trouvant les différences de variabilité interannuelle pour différentes variables de surface et atmosphériques, qui pourraient potentiellement contribuer à relier l'humidité du sol à la température de l'air. Celles-ci incluent la profondeur de la neige, l'albédo de surface, le pourcentage d'eau liquide dans le sol, le rayonnement net à la surface, le rayonnement long sortant, le flux de chaleur latente, et la température du sol.

Pour analyser l'effet de la variabilité de l'humidité du sol sur les températures extrêmes, le 90^e centile de la température maximale journalière est utilisée comme critère de sélection pour qualifier une journée chaude. Les nombres de journées chaudes dans les observations, les simulations couplées et non-couplées sont ensuite comparées.

Enfin, pour étudier les changements dans le couplage sous l'effet du réchauffement climatique, des simulations couplées et non-couplées sont réalisées avec MRCC5, piloté par le MGC, Canadian Earth System Model (CanESM2) [Arora *et al.*, 2011]. Des périodes de 30 ans allant de 1981 à 2010 et de 2071 à 2100 sont utilisées pour comparer le climat actuel et futur. Pour la période de 2071 à 2100, des scénarios représentatifs (RCP 4,5 et 8,5) d'évolution de la concentration de gaz à effet de serre sont utilisés. Ces scénarios mènent à des forçages radiatifs nets de + 4,5 et + 8,5 W/m² respectivement. L'intensité et les mécanismes du couplage dans le futur sont calculés en utilisant les même méthodes mentionnées ci-haut.

1.3 Organisation du mémoire

Le premier chapitre comprend l'introduction, qui est divisée en deux parties : la problématique et les objectifs, et la méthodologie. Le reste du mémoire est organisé en deux chapitres supplémentaires. Le deuxième chapitre est présenté sous forme d'article rédigé en anglais. Cet article est divisé en quatre sections : l'introduction, la description du modèle MRCC5 et des méthodes utilisées, les résultats obtenus pour l'analyse du couplage dans MRCC5, et les conclusions. Le troisième chapitre comporte une discussion des résultats et des conclusions plus approfondies rédigées en français.

CHAPITRE II

THE INTER- AND INTRA-SEASONAL VARIABILITY OF LAND-ATMOSPHERE COUPLING OVER NORTH AMERICA IN THE FIFTH GENERATION CANADIAN REGIONAL CLIMATE MODEL (CRCM5)

Gregory Yang Kam Wing*, Laxmi Sushama and Gulilat Tefera Diro

Centre ESCER, Département des sciences de la terre et de l'atmosphère,
Université du Québec à Montréal, Montréal, QC, Canada

* Corresponding author : Gregory Yang Kam Wing

Centre ESCER,

Département des sciences de la terre et de l'atmosphère

Université du Québec à Montréal

201 Avenue Président Kennedy (PK-6415)

Montréal, QC H2X 3Y7

Canada

E-mail : yang@sca.uqam.ca

Submitted to Journal of Geophysical Research : Atmospheres

Abstract

This study investigates the inter- and intra-seasonal variability of soil moisture-temperature coupling for the mid- to high-latitude regions of North America. To this effect, coupled and uncoupled simulations are performed with the fifth-generation Canadian Regional Climate Model (CRCM5). In coupled simulations, the land and the atmosphere interact freely ; in uncoupled simulations, the interannual variability of soil moisture is suppressed by prescribing soil liquid and frozen water contents with climatological values. The study also explores projected changes to coupling by comparing coupled and uncoupled simulations for current (1981–2010) and future (2071–2100) periods.

Results show that coupling, in the current climate, is strong from the southern US Great Plains to the southern Canadian Prairies. While coupling over the Great Plains is persistent throughout the year, coupling over the Prairies follows the seasonal evolution of the freezing line. Analysis of coupling over the Prairies for spring and fall reveals an underlying mechanism different from that of the better-studied summer season : soil water phase and snow depth alter the surface albedo, which affects the net shortwave and upwelling longwave radiations and therefore air temperature. For regions with strong coupling, coupled simulations reflect observed extreme temperatures reasonably well, and produce a higher number of hot days than uncoupled simulations. This suggests that soil moisture variability can amplify the frequency of temperature extremes. In the projected future climate, changes in coupling are season-specific : drier soil conditions strengthen coupling during summer, while changes in snow depth and cloud cover influence coupling during spring and fall.

Keywords : soil moisture, land-atmosphere coupling, North America, regional climate model, climate change, temperature extremes

2.1 Introduction

Land plays an important role in the climate system. Land surface state, particularly soil moisture, can influence the atmosphere. *Koster et al.* [2004], within the framework of the Global Land-Atmosphere Coupling Experiment (GLACE), studied land-atmosphere coupling, using highly controlled simulations that were performed with 12 Global Climate Models (GCMs). They quantified the impact of soil moisture variability on atmospheric variability, and developed a global map showing regions where soil moisture variability has the strongest effect on temperature and precipitation variability during boreal summer. The 12 GCMs indicated that land-atmosphere coupling is important over transitional zones between dry and wet climates, i.e. regions where evapotranspiration is limited by soil moisture. However, a large spread in the coupling strengths was reported in the studied models. As discussed in *van den Hurk et al.* [2011], the important differences between the model results presented in *Koster et al.* [2004] demonstrate the intricacy of land-atmosphere coupling, and the need for more model intercomparison studies due to the uncertainties caused by different physical parameterizations in the models. Recently, there has also been an increase in the number of land-atmosphere coupling experiments mainly because it has been shown that significant anomalies in soil moisture, can contribute to the amplification and persistence of regional-scale extreme events, such as heatwaves, droughts and floods [*Oglesby and Erickson*, 1989; *Beljaars et al.*, 1996; *Betts*, 2004; *Fischer et al.*, 2007a,b].

Due to their higher resolution, Regional Climate Models (RCMs) have the ability to better represent surface heterogeneity, which can be an important factor in determining the land surface state, particularly soil moisture and therefore regions of strong land-atmosphere coupling (coupling hotspots), which GCMs may not capture. For instance, using the Climate High-Resolution Model (CHRM) [*Vidale et al.*, 2003], *Seneviratne et al.* [2006] observed strong soil moisture-temperature coupling over the Mediterranean region in Europe, a transitional zone between dry and wet climates that was not iden-

tified as a coupling hotspot in GLACE. Besides, while the Great Plains have been identified as a coupling hotspot over North America in GLACE, additional coupling hotspots were found in experiments performed with RCMs. For example, using the fifth-generation Canadian Regional Climate Model (CRCM5), *Diro et al.* [2014] observed strong coupling over southeastern and northwestern US, wet and dry regions respectively that become transitional zones where atmospheric variability becomes sensitive to soil moisture under extreme conditions. In addition, *Zhang et al.* [2008], using the second version of the Weather Research and Forecasting (WRF) model [*Skamarock et al.*, 2005], found that strong coupling could actually be observed over a much larger area of the United States than what was reported by *Koster et al.* [2004], spanning from the southwest, to the Northern Great Plains, and to the southeast. This is because coupling is not only sensitive to soil moisture, but also to the air temperature regime, particularly the air temperature range, which may be better resolved in RCMs than in GCMs. *Zhang et al.* [2008] report that coupling is stronger in the 23–29°C range when air temperature is not too low to limit the impact of sensible heat flux, and not too high to completely dry out the soil and suppress the influence of soil moisture. Nonetheless, results from some experiments with RCMs remain consistent with the findings of GLACE. For instance, using the International Center for Theoretical Physics (ICTP) Regional Climate Model version 4.0 (RegCM4.0) [*Giorgi et al.*, 2012], *Mei et al.* [2013] adopted similar methods to *Koster et al.* [2004], enabling them to also identify the US Great Plains as the most significant coupling hotspot over North America during boreal summer.

It is well established that soil moisture influences air temperature via the partitioning of net surface radiation into turbulent heat fluxes during summer [*Pal and Eltahir*, 2001]. However, the soil moisture-temperature coupling mechanism has not been as well explored for the other seasons. In a recent study using ICTP's Regional Climate Model (RegCM) [*Pal et al.*, 2007], coupled with the National Center for Atmospheric Research (NCAR) Community Land Model (CLM) version 3.5 [*Oleson et al.*, 2008],

Tawfik and Steiner [2011] observed that soil moisture-temperature coupling over the US Great Plains is especially strong during the spring and fall seasons. They also demonstrated that the location of maximum coupling strength follows the seasonal evolution of the freezing line, and identified soil water phase, i.e. the fractional soil liquid and frozen water contents, as the main factor behind this coupling.

Furthermore, while the aforementioned studies have only considered the current climate, few studies have investigated soil moisture-temperature coupling for the summer season in future climate. *Seneviratne et al.* [2006] reported that the location of soil moisture-temperature coupling hotspots could shift northward from the Mediterranean region to Central and Eastern Europe in future climate. Moreover, in their study over North America, *Diro and Sushama* [2016] reported that soil moisture-temperature coupling hotspots could expand further north in future climate. In both studies, enhanced coupling strength in more northern regions were associated with relatively drier soil conditions in the future climate compared to the current climate, leading to soil moisture-limited rather than energy-limited evapotranspiration. Nevertheless, these results only provide information about future changes of soil moisture-temperature coupling for the summer season but not for other seasons.

This study therefore focuses on the inter- and intra-seasonal variability of soil moisture-temperature coupling over North America using CRCM5. The objectives are twofold. The first is to investigate the seasonal differences in the strength and underlying mechanisms of soil moisture-temperature coupling, and the impact of soil moisture variability on temperature extremes in current climate. The second is to study projected changes to the above in a future warmer climate. To address these questions, simulations with and without soil moisture-temperature coupling are performed with CRCM5 over North America. In the coupled simulations, soil moisture interacts freely with the atmosphere. In the uncoupled simulations, soil liquid and frozen water contents are prescribed with climatological values at every timestep, thereby suppressing the interannual variability

of soil moisture. The strength of soil moisture-temperature coupling can therefore be evaluated by comparing these simulations.

The rest of the article is organized as follows : a brief description of the model and methods is given in Section 2.2, comparisons of the coupled and uncoupled simulations for various seasons in the current climate are discussed in Section 2.3, projected changes to coupling are described in Section 2.4, and conclusions are presented in Section 2.5.

2.2 Model, methods and observational data

2.2.1 Model

The regional climate model used in this study, CRCM5 [Zadra *et al.*, 2008], is based on a limited-area version of the Global Environment Multiscale (GEM) model [Côté *et al.*, 1998], which employs semi-Lagrangian transport and an almost fully implicit stepping scheme [Martynov *et al.*, 2013]. In its completely elastic non-hydrostatic formulation [Yeh *et al.*, 2002], GEM uses a vertical coordinate based on hydrostatic pressure [Laprise, 1992]. The physical parameterizations in CRCM5 that were adapted from GEM include : deep convection based on Kain and Fritsch [1990], shallow convection based on a transient version of the Kuo [1965] scheme [Bélair *et al.*, 2005], large-scale condensation [Sundqvist *et al.*, 1989], correlated-K solar and terrestrial radiations [Li and Barker, 2005], subgrid-scale orographic gravity-wave drag [McFarlane, 1987], turbulent kinetic energy closure in the planetary boundary layer, and vertical diffusion [Benoit *et al.*, 1989; Delage and Girard, 1992; Delage, 1997]. In CRCM5, lakes are represented using the 1-D Flake model [Martynov *et al.*, 2010, 2012]. To provide an explicit representation of vegetation and land-surface types, CRCM5 uses the latest version of the Canadian Land Surface Scheme (CLASS v3.5) [Versegny, 1991; Versegny *et al.*, 1993; Versegny, 2011]. A deep soil configuration, consisting of 26 layers for a total depth of 60 meters, and a spatially varying depth to bedrock, derived from Webb

et al. [2000], are used. CLASS includes prognostic equations for energy and water conservation for the soil layers and a thermally and hydrologically distinct snow pack where applicable. The thermal budget is accounted for in all layers, but the hydrological budget is only considered for layers above the bedrock. In an attempt to crudely mimic subgrid-scale variability, CLASS adopts a pseudomosaic approach and divides the land fraction of each grid cell into a maximum of four subareas : bare soil, vegetation, snow over bare soil, and snow with vegetation. The energy and water budget equations are first solved for each subarea separately and then averaged over the grid cell.

2.2.2 Methods and observational data

The coupled and uncoupled simulations considered in this study are performed using CRCM5 at 0.44° ($\sim 50\text{km}$) horizontal resolution with a 20-minute time step over a domain covering North America. This integration domain consists of 212×200 grid points. The outer 20 grid points are used for nesting : the 10 outermost grid points, which are either driven by reanalysis or a GCM, provide upstream data for semi-Lagrangian interpolation, and the 10 innermost grid points act as a buffer zone in which the atmospheric variables of CRCM5 are damped towards the driving fields [Martynov *et al.*, 2013]. The remaining inner 172×160 grid points, covering North America between 20°N – 88°N and 30°W – 150°W , is the free zone considered for analysis.

CRCM5's ability in reproducing variables that are relevant to this study, such as the two-meter temperature, snow depth and surface albedo, is first evaluated by comparing model outputs with available observational datasets. Monthly gridded data from the Climatic Research Unit (CRU TS3.10) at University of East Anglia [Harris *et al.*, 2014] is used for validating the seasonal mean and interannual variability of two-meter temperature for the 1981–2010 period. This dataset has a 0.5° spatial resolution and is based on meteorological station observations over land. Surface albedo in CRCM5 is validated against monthly data obtained from NASA's International Satellite Cloud Climatology

Project (ISCCP) [Rossow and Schiffer, 1999]. The ISCCP dataset is available at 2.5° spatial resolution and is based on weather satellite observations. To validate snow depth in CRCM5, daily snow depth records are obtained from the Canadian Meteorological Centre (CMC) [Brown *et al.*, 2003]. The CMC dataset is available at 0.25° spatial resolution and is derived from weather station observations.

Soil moisture-temperature coupling for the current 1981–2010 period is assessed by comparing coupled and uncoupled CRCM5 simulations, driven by ERA-40 reanalyses [Uppala *et al.*, 2005] for the 1958–1978 period and ERA-Interim reanalyses [Dee *et al.*, 2011] for the 1979–2010 period. In the uncoupled simulation, soil frozen and liquid water contents are prescribed with climatological averages, obtained from the coupled simulation, at every time step. This suppresses the interannual variability of soil moisture. As described in Table 2.1, these simulations will be referred to as CRCM5 – ERA ; the subscripts ‘coupled’ and ‘uncoupled’ will be added when it is necessary to specify which type of simulation is being referred to.

Since the only difference between coupled and uncoupled simulations is the interannual variability of soil moisture, comparing these simulations reveals the extent to which soil moisture variability affects atmospheric variability. The soil moisture-temperature coupling strength is therefore assessed using the standard deviation difference method following Tawfik and Steiner [2011], which is defined as :

$$\Delta\sigma_T = \sigma_{T,coupled} - \sigma_{T,uncoupled} \quad (2.1)$$

where $\sigma_{T,coupled}$ and $\sigma_{T,uncoupled}$ are the interannual variability of two-meter temperature from the coupled and uncoupled simulations respectively.

The underlying mechanisms that lead to soil moisture-temperature coupling in various seasons are also assessed by studying the differences in interannual variability between coupled and uncoupled simulations for relevant surface and atmospheric variables, such

as snow depth, surface albedo, fraction of soil liquid water, net shortwave radiation, upwelling longwave radiation, downwelling longwave radiation, latent heat flux, soil temperature, and cloud cover. Moreover, the influence of soil moisture variability on temperature extremes is investigated by comparing the spatial distribution of the number of hot days in the coupled and uncoupled simulations with those observed for the 1981–2010 period. In this study, a hot day is defined as a day with maximum temperature above the 90th percentile of daily maximum temperatures. This threshold, which is different for each grid point and for each day, is calculated from the coupled simulations, and is used in determining the number of hot days for both coupled and uncoupled simulations.

Finally, to study the projected changes to soil moisture-temperature coupling, transient climate change coupled CRCM5 simulations, spanning the 1950–2100 period, are considered. These simulations are driven by the second-generation Canadian Earth System Model (CanESM2) [Arora *et al.*, 2011] for RCPs 4.5 and 8.5, which are scenarios that were implemented by the Intergovernmental Panel on Climate Change (IPCC) in its fifth Assessment Report (AR5), and represent increases in greenhouse gas emissions throughout the 21st century, leading to net radiative forcings of +4.5 and +8.5 W/m² respectively [Moss *et al.*, 2008 ; Riahi *et al.*, 2011]. It must be noted that the 1950–2005 periods are exactly the same for these simulations. For analysis purposes, only the 2071–2100 and 1981–2010 periods are considered in this study. The mean soil moisture for the 2071–2100 period is different from that for the 1981–2010 period. For these two 30-year time periods, the uncoupled CanESM2-driven CRCM5 simulations are therefore also performed by prescribing soil moisture with the respective climatological averages. As described in Table 2.1, CanESM2-driven CRCM5 simulations will be referred to as CRCM5 – CanC for the 1981–2010 period, and CRCM5 – CanRCP4.5 and CRCM5 – CanRCP8.5 for the 2071–2100 period for RCPs 4.5 and 8.5 respectively ; the subscripts ‘coupled’ and ‘uncoupled’ will be added to the names as required.

2.3 Soil moisture-temperature coupling in current climate

2.3.1 Model evaluation

Comparison of CRCM5 – ERA_{coupled} and CRU suggests that the model captures reasonably well the spatial patterns of mean seasonal two-meter temperatures [Figure 2.1a]. On average, differences between the modeled and observed mean seasonal two-meter temperatures are below $\pm 2^{\circ}\text{C}$, except during spring (MAM) when an underestimation of up to -3°C is noted over Alaska and the boreal forest region. This could be due to an overestimation of snow depth [Figure 2.2a], which leads to an overestimation of surface albedo [Figure 2.3a]. There are several possible reasons that could explain the discrepancy noted between the modeled and observed mean snow depths over these regions for the spring season. First, the lack of observations over the coast mountains in Alaska could contribute to uncertainties in the observational data. As also reported by *Martynov et al.* [2013], the higher snow depth values simulated in the model compared to observations could be associated with an overestimation of winter precipitation. In addition, the model's overestimation of snow depth over a few grid cells could be the result of an inadequate representation of the transformation of snow into glaciers. Moreover, the cooler temperatures noted over the boreal forest region could be related to the overestimation of surface albedo itself, which is partly due to the inadequate parameterization of the unloading of snow intercepted by vegetation [Bartlett and Versegny, 2015].

During spring and winter (DJF), CRCM5 – ERA_{coupled} also exhibits a cold bias over the southern part of the Canadian Prairies. According to the vegetation dataset used in the model, the grid cells covering the Canadian Prairies are almost entirely croplands. These grid cells will therefore be treated as bare soil, with or without snow as the case may be, during the period between harvest and the beginning of the growing season in late spring the following year. This leads to an overestimation of surface albedo, and subsequently cooler temperatures. Compared to CRU, the spatial patterns of the interannual

variability of two-meter temperature are also well represented in CRCM5 – ERA_{coupled} [Figure 2.1b]. During spring, however, CRCM5 – ERA_{coupled} has a positive bias in this interannual variability over the Canadian Prairies. This appears to be linked to the overestimation of the interannual variability of surface albedo [Figure 2.2b], which is caused by an overestimation of the interannual variability of snow depth [Figure 2.3b].

It must be noted that snow depth for the high Arctic region is mostly overestimated, but the reliability of the observation data is also questionable for these regions. Despite the overestimation in snow depth for these regions, the surface albedo values appear reasonable compared to ISCCP.

2.3.2 Coupling strength and underlying mechanisms

Figure 2.4a shows the monthly soil moisture-temperature coupling strengths over North America in CRCM5 – ERA. The months of January and February are not shown as snow covers almost half the continent, thus uncoupling the soil from the atmosphere. Strongest coupling is observed over the region spanning from the southern US Great Plains to the southern Canadian Prairies, which is a transition zone between dry and wet climates where evapotranspiration is soil moisture-limited [Koster *et al.*, 2004; Diro *et al.*, 2014]. The southern part of this coupling hotspot is more or less persistent throughout the year, with maximum coupling strength occurring during spring and summer, as expected.

Over the northern part, coupling exhibits an interesting behavior. Strong coupling observed south of the Canadian Prairies in March, migrates northward during April, and is situated over the southern Canadian Prairies in May. In June and July, strong coupling is observed not only over the southern Canadian Prairies but also over the northern regions of Canada where the increase in solar insolation during summer leads to an increase in evapotranspiration. Starting October, regions of strong coupling start mi-

grating southward, and another peak in coupling strength is observed over the southern Canadian Prairies in November. It should be noted that the boreal forest region, in between the southern Canadian Prairies and northern regions of Canada, constantly shows weak coupling. This is because evapotranspiration over these regions is energy-limited rather than soil moisture-limited.

During the March to November period, coupling is particularly strong over the region between 115°W – 95°W and 48°N – 58°N , which covers the southern Canadian Prairies (shown enclosed by the small rectangle in Figure 2.4a). This is clearly visible in the zonally averaged monthly coupling strengths for this region, shown in Figure 2.4b. The agriculture sector is very important for the southern Canadian Prairies. As crops are vulnerable to extreme climatic conditions including temperature extremes [Herrington *et al.*, 1997; Luciuk and O'Brien, 1999; Cohen and Miller, 2001; Bradshaw *et al.*, 2004], it is important to have a better understanding of the coupling process, which can amplify these extreme conditions. Therefore, further analysis is performed to identify the mechanisms responsible for the weakening and strengthening of coupling between seasons over this region. The northward and southward migrations of maximum coupling strength during spring and fall, with the freezing line, suggests that periods of soil thawing and freezing could act as an important driver of the land-atmosphere feedback mechanism during these seasons. This is reflected in the monthly interannual variability of soil liquid water fraction in CRCM5 – ERA_{coupled} [Figure 2.5a], with maximum variability migrating northward from February to June and southward from October to December. Up to this point, Tawfik and Steiner [2011] obtained similar results for a more southern location that was mainly comprised of the northern US Great Plains. However, the high values in the interannual variability of soil liquid water fraction over the Prairies, which are observed here, translate into large differences in interannual variability between coupled and uncoupled simulations for variables that were not considered in their study.

High variability in soil liquid water fraction over the Prairies is first found to be collocated with large differences in snow depth variability between 54°N and 58°N in May and June, and between 48°N and 52°N in March, April and November [Figure 2.5b]. This is expected since snow acts as a thermal insulator, thereby regulating soil thawing and freezing. In addition, more frozen soil can contribute to cooler land surface temperatures and thus delay snowmelt. It must be noted that the snow depth variability is in general weaker for the boreal forest region, roughly situated between 52°N and 54°N. Both the soil water phase and snow depth influence the surface albedo, and this is reflected in Figure 2.5c with high values of the variability of surface albedo collocated with high values of the variability of snow depth and soil liquid water fraction.

The variability of surface albedo, along with the variability of cloud cover [Figure 2.5d], is reflected in the variability of net shortwave radiation [Figure 2.5e], and therefore in the variability of soil temperature [Figure 2.5f] and upwelling longwave radiation [Figure 2.5g], which explains the larger interannual variability of two-meter temperature observed during spring and fall. The signals obtained for the variability in the turbulent heat fluxes are strong during summer but not as obvious during spring and fall. This is because evapotranspiration is soil moisture-limited in summer but mostly energy-limited in spring and fall. Nevertheless, high latent heat flux variability is collocated with high two-meter temperature variability during spring, albeit to a lesser extent compared to the upwelling longwave radiation variability [Figure 2.5h]. Results also suggest that the temperature variability influences the snow depth variability, which can then influence the surface albedo variability through a feedback loop.

2.3.3 Influence of soil moisture variability on temperature extremes

The influence of soil moisture variability on temperature extremes is evaluated by comparing the number of hot days in coupled and uncoupled CRCM5 – ERA simulations. As mentioned before, a hot day is defined as a day with daily maximum temperature

exceeding the 90th percentile of maximum temperature for the respective day. This threshold is calculated for each grid point from the coupled simulation and used to determine the number of hot days in both coupled and uncoupled simulations.

Before calculating the number of hot days in coupled and uncoupled simulations, the ability of CRCM5 – ERA_{coupled} in reproducing the monthly means of the 90th percentiles of daily maximum temperatures is evaluated using daily gridded data obtained from *Xia et al.* [2012] for the US, and *Hutchinson et al.* [2009] and *Hopkinson et al.* [2011] for Canada below 60°N. In general, the spatial distribution of the 90th percentiles is well reproduced by CRCM5 – ERA_{coupled} compared with observations [Figure 2.6a]. Differences between modeled and observed 90th percentiles are below $\pm 3^{\circ}\text{C}$ during winter and fall, but exceed $\pm 5^{\circ}\text{C}$ over certain locations during spring and summer [Figure 2.6b]. In March and April, for example, CRCM5 – ERA_{coupled} underestimates the 90th percentile over the southern Canadian Prairies and northern Québec. As mentioned before, this could be associated with an overestimation of surface albedo, caused by an overestimation of snow depth. Additionally, CRCM5 – ERA_{coupled} overestimates the 90th percentile over Midwestern US in July and August. As reported by *Diro et al.* [2014], precipitation over this region is also underestimated in CRCM5 – ERA_{coupled} compared to observations. Lower precipitation is associated with lower cloud cover and therefore more incoming solar radiation, leading to warmer temperatures.

Figure 2.6c shows the monthly differences in the mean number of hot days between CRCM5 – ERA_{coupled} and CRCM5 – ERA_{uncoupled}. As expected, the area spanning from the southern US Great Plains to the southern Canadian Prairies is the region where soil moisture variability has the greatest impact on the number of hot days. Over this region, soil moisture variability amplifies the monthly number of hot days by 2 to 3 days. It should be noted that the underestimation of the 90th percentile over this region, as discussed above, could lead to a lower estimate of the number of hot days. This suggests that soil moisture variability could in fact have an even greater impact on temperature

extremes over this region, should the 90th percentile have been better represented in the model. Similar to the coupling strength, the influence of soil moisture variability on the number of hot days over the southern US Great Plains remains persistent throughout the year, with maximum differences in the number of hot days observed during the summer months. Over the southern Canadian Prairies, on the other hand, the location of the maximum difference in the number of hot days follows the freezing line : it migrates northward from March to August and southward from September to December. In particular, peak values in the difference in the number of hot days are noted in May and October, which are months when maximum coupling strengths are observed [Figure 2.4b]. Besides, with the increase in solar insolation and the progression of the freezing line, the number of hot days over northern regions of Canada during summer is also amplified by soil moisture variability to some extent.

2.4 Projected changes to soil moisture-temperature coupling

2.4.1 Coupling strength and underlying mechanisms

The projected changes to soil moisture-temperature coupling are assessed by comparing CRCM5 – CanC with CRCM5 – CanRCP4.5 and CRCM5 – CanRCP8.5. Prior to that, the boundary forcing errors due to errors in the driving CanESM2 data are studied by comparing CRCM5 – CanC with CRCM5 – ERA for the current climate. In general, the location of the coupling hotspots over North America in CRCM5 – CanC is similar to that in CRCM5 – ERA, with the strongest coupling observed over the region spanning from the southern US Great Plains to the southern Canadian Prairies [Figure 2.7a]. Moreover, the seasonal evolution of maximum coupling strength following the freezing line, which was observed in CRCM5 – ERA for the northern part of this region, is well represented in CRCM5 – CanC. However, there are some differences in coupling strength over this region between CRCM5 – ERA [Figure 2.4b] and CRCM5 – CanC [Figure 2.7b], particularly during spring and fall. To explain these differences in cou-

pling strength, the differences in interannual variability between coupled and uncoupled simulations for snow depth, cloud cover and net shortwave radiation are studied [Figure 2.8]. Compared to CRCM5 – ERA, maximum coupling strength in CRCM5 – CanC is shifted from May to April between 54°N and 58°N, and from March to April between 48°N and 54°N during spring. This is associated with earlier and delayed snowmelt in CRCM5 – CanC over the higher and lower latitudes respectively. As snowmelt occurs predominantly in April in CRCM5 – CanC, smaller differences in snow depth variability between coupled and uncoupled simulations are also obtained in CRCM5 – CanC compared to CRCM5 – ERA for March and May [Figure 2.8a]. During fall, the later onset of snow accumulation between 48°N and 52°N in CRCM5 – CanC has the same impact as the earlier spring snowmelt observed at the lower latitudes, leading to smaller differences in snow depth variability between coupled and uncoupled simulations in CRCM5 – CanC compared to CRCM5 – ERA for November. For this season, the differences in cloud cover variability between coupled and uncoupled simulations have an additional impact on coupling strength. While these differences are comparable in CRCM5 – CanC and CRCM5 – ERA for October, they are relatively lower in CRCM5 – CanC compared to CRCM5 – ERA for November [Figure 2.8b]. The smaller differences of snow depth and cloud cover variability, which are produced in CRCM5 – CanC with respect to CRCM5 – ERA, appear to translate into smaller differences of net shortwave radiation variability [Figure 2.8c], which then lead to smaller differences in two-meter temperature variability, i.e. weaker soil moisture-temperature coupling, via the same mechanisms that were discussed in section 2.3.2.

In the future climate, the general soil moisture-temperature coupling patterns for both RCPs 4.5 and 8.5 are similar to that of the current climate [Figures 2.9a and 2.10a]. As in CRCM5 – CanC, the region spanning from the southern US Great Plains to the southern Canadian Prairies is the area that exhibits strongest coupling over North America in both CRCM5 – CanRCP4.5 and CRCM5 – CanRCP8.5. However, when further

analysis is performed for the northern part of this region, particularly the area enclosed by 115°W–95°W and 48°N–58°N, differences in coupling during spring, summer and fall [Figures 2.9b and 2.10b] are observed due to modifications in the differences in interannual variability for snow depth, cloud cover, downwelling longwave radiation, soil ice, and soil liquid water fraction [Figure 2.11].

During spring, the differences in interannual variability between coupled and uncoupled simulations for snow depth [Figure 2.11a] appear to be associated with the changes in soil moisture-temperature coupling strength observed in CRCM5 – CanRCP8.5. In both CRCM5 – CanC and CRCM5 – CanRCP4.5, large differences in snow depth variability are observed mainly in April. In CRCM5 – CanRCP8.5, on the other hand, the maximum difference in snow depth variability is shifted from April to March. This could be due to earlier snowmelt, which is associated with warmer surface temperatures caused by a reduction in soil frozen water content in CRCM5 – CanRCP8.5 as opposed to the other two simulations. This leads to a shift in the maximum difference in surface albedo variability [Figure 2.11b], and ultimately a shift in maximum coupling strength from April to March in CRCM5 – CanRCP8.5.

During fall, larger differences in interannual variability between coupled and uncoupled simulations for downwelling longwave radiation [Figure 2.11c] appear to be related to the stronger soil moisture-temperature coupling exhibited by CRCM5 – CanRCP8.5 in November compared to CRCM5 – CanC and CRCM5 – CanRCP4.5. Differences in downwelling longwave radiation variability play a greater role in CRCM5 – CanRCP8.5 than in CRCM5 – CanC because of differences in cloud cover variability between the two simulations. In particular, higher cloud cover variability is observed in CRCM5 – CanRCP8.5_{coupled} compared to CRCM5 – CanC_{coupled} [Figure A1]. Since greenhouse gas concentrations are higher in CRCM5 – CanRCP8.5 than in CRCM5 – CanRCP4.5, the differences in downwelling longwave radiation variability are also higher in CRCM5 – CanRCP8.5 than in CRCM5 – CanRCP4.5. This is because greenhouse gases can play

a minor role in amplifying the contribution of cloud cover to downwelling longwave radiation. In CRCM5 – CanRCP8.5, the influence of soil moisture variability on the cloud cover variability therefore plays a more important role in the soil moisture-temperature coupling process compared to CRCM5 – CanC and CRCM5 – CanRCP4.5. Cloud cover affects the downwelling longwave radiation, which then influences soil temperature, and the two-meter temperature via upwelling longwave radiation. Hence, the larger differences in downwelling longwave radiation variability eventually lead to stronger soil moisture-temperature coupling in CRCM5 – CanRCP8.5 for November.

Differences in the mean soil frozen water content are also responsible for the difference in soil moisture-temperature coupling strength between CRCM5 – CanRCP8.5 and CRCM5 – CanRCP4.5 in November. To explain this, the decreases in the mean soil frozen water content in CRCM5 – CanRCP8.5_{coupled} and CRCM5 – CanRCP4.5_{coupled} with respect to CRCM5 – CanC are studied [Figure A2]. Although the mean soil frozen water content is lower with respect to CRCM5 – CanC_{coupled} in both simulations, a larger decrease in the mean soil frozen water content can be observed in CRCM5 – CanRCP8.5_{coupled} compared to CRCM5 – CanRCP4.5_{coupled}. Less frozen water in the soil implies more liquid water in the soil, warmer soil temperatures and greater upwelling longwave radiation, which leads to warmer two-meter temperatures. Hence, the larger decrease in the mean soil frozen water content in CRCM5 – CanRCP8.5_{coupled} leads to larger differences in interannual variability between coupled and uncoupled simulations for two-meter temperature in CRCM5 – CanRCP8.5 compared to CRCM5 – CanRCP4.5.

During summer, an increase in soil moisture-temperature coupling strength is noted in both CRCM5 – CanRCP4.5 and CRCM5 – CanRCP8.5 compared with CRCM5 – CanC. This is because of decreases in soil liquid water content, which are caused by decreases in precipitation rates in both CRCM5 – CanRCP4.5_{coupled} and CRCM5 – CanRCP8.5_{coupled} with respect to CRCM5 – CanC_{coupled} [Figure A3]. This is consistent

with studies by Šeparović *et al.* [2013], and Diro and Sushama [2016], which reported decreases in precipitation rates over the region spanning from the southern Great Plains to the southern Canadian Prairies in future climate using CanESM2-driven CRCM5 simulations. The drier soil state in the future compared to the current climate transforms the southern Canadian Prairies into a transitional zone where evapotranspiration is soil moisture-limited rather than energy-limited, resulting in greater soil moisture-temperature coupling strength during the summer season.

2.4.2 Influence of soil moisture variability on temperature extremes

To determine the changes in the influence of soil moisture variability on the number of hot days in future climate, the monthly means of the 90th percentiles of daily maximum temperatures in CRCM5 – CanC_{coupled} are first compared with the same daily gridded observational datasets used in section 2.3.3. Compared to CRCM5 – ERA_{coupled}, CRCM5 – CanC_{coupled} underestimates the 90th percentile of daily maximum temperature over most of the North American continent during the colder months, especially over the southern Canadian Prairies and northern Québec in March and April [Figure 2.12a]. This is partly due to an overestimation of surface albedo, caused by an overestimation of snow depth in CRCM5 – CanC_{coupled}. Despite these biases, the northward and southward migration of regions with maximum differences in the number of hot days between coupled and uncoupled simulations, which are observed in CRCM5 – ERA_{coupled}, are well captured by CRCM5 – CanC_{coupled} [Figure 2.12b]. Compared with CRCM5 – ERA, the maximum differences in the number of hot days over the southern Canadian Prairies are also observed at more or less the same time in CRCM5 – CanC, particularly during summer and in October. However, the peak difference in May, which was observed over this region in CRCM5 – ERA, is not reproduced in CRCM5 – CanC. This is consistent with the weaker coupling strength observed in May in CRCM5 – CanC with respect to CRCM5 – ERA, as discussed in section 2.4.1.

Figure 2.13 shows the monthly differences in the mean number of hot days between coupled and uncoupled simulations for CRCM5 – CanRCP4.5 and CRCM5 – CanRCP8.5. Compared to CRCM5 – CanC, the differences in soil moisture variability between coupled and uncoupled simulations amplify the differences in the number of hot days over a much larger area zonally, especially during summer, in both CRCM5 – CanRCP4.5 and CRCM5 – CanRCP8.5. This is due to relatively drier soil conditions, which prevail over most of the North American continent in the future climate, leading to more soil moisture-limited rather than energy-limited evapotranspiration. Moreover, the timing of the northward and southward migrations of regions with maximum differences in the number of hot days between coupled and uncoupled simulations are shifted with respect to the current climate. This is associated with differences in the timing of snowmelt during spring and snow accumulation during fall. Consequently, in both CRCM5 – CanRCP4.5 and CRCM5 – CanRCP8.5, the initial northward migration starts earlier during spring due to earlier snowmelt, and the final southward migration occurs later during fall due to delayed snow accumulation compared to CRCM5 – CanC.

2.5 Summary and conclusions

In this study, soil moisture-temperature coupling over North America is analyzed by comparing coupled with uncoupled simulations, performed with CRCM5. In the uncoupled simulation, the interaction between soil moisture and temperature is inhibited by prescribing soil frozen and liquid water content with climatological means at every time step. As this modification suppresses the interannual variability of soil moisture, the difference between coupled and uncoupled simulations reveals the extent to which soil moisture variability influences temperature variability. Compared to observations, the ERA-driven CRCM5 simulation is a good representation of the observed spatial distribution of the seasonal mean and interannual variability of two-meter temperature, snow depth and surface albedo, which are variables that are relevant to soil

moisture-temperature coupling. This confirms the suitability of the model for studying the seasonal evolution of soil moisture-temperature coupling. It should be noted that soil moisture in CRCM5 could not be validated because of the lack of observational data.

Analysis shows that soil moisture-temperature coupling is strongest over the region extending from the southern US Great Plains to the southern Canadian Prairies. The southern part of this hotspot is more persistent : it reaches peak intensity during summer whilst remaining at a more or less fixed location throughout the year. Coupling over the northern part of this hotspot, on the other hand, evolves in a similar way to the freezing line during spring and fall, implying that soil water phase plays an important role in modulating soil moisture-temperature coupling during transition periods. This result is consistent with the findings of *Tawfik and Steiner* [2011], but their focus was on a more southern location that mainly included the northern US Great Plains. Here, analysis of the underlying mechanisms of soil moisture-temperature coupling over the northern part of the hotspot, with a particular focus on the southern Canadian Prairies, reveals that soil water phase and snow depth variability both influence surface albedo variability. This in turn affects the absorbed shortwave and emitted longwave radiations. The high variability of upwelling longwave radiation, in particular, may be linked to the high variability in two-meter temperature observed during spring and fall. The two-meter temperature variability then appears to translate into the snow depth variability, which affects both the surface albedo and soil moisture through a feedback loop.

Important changes in soil moisture-temperature coupling over the southern Canadian Prairies are noted for the future climate due to season-specific differences in snow depth, soil moisture, and downwelling longwave radiation. During spring, earlier snowmelt leads to a shift in the timing of maximum coupling strength. During summer, evapotranspiration becomes more soil moisture-limited due to relatively drier soil conditions, leading to stronger coupling, and during fall, increased cloud cover leads to a greater

influence of downwelling longwave radiation on the two-meter temperature.

Further analyses also reveal that soil moisture variability indeed amplifies temperature extremes, particularly the number of hot days, in the same locations where strong soil moisture-temperature coupling is observed in the current climate. In the future climate, regions of strong soil moisture-temperature coupling cover a much wider region over North America and hence, the influence of soil moisture variability on the number of hot days spans over a larger area zonally, especially for RCP 8.5. Such events could be particularly disastrous to agricultural regions, such as the southern Canadian Prairies, because some crops cannot adapt easily to sudden changes in climate [*Herrington et al.*, 1997 ; *Luciuk and O'Brien*, 1999 ; *Cohen and Miller*, 2001 ; *Bradshaw et al.*, 2004]. This shows that a better understanding of the mechanisms of soil moisture-temperature coupling should be acquired to improve the ability to forecast such events.

Although this study covers several aspects of the influence of soil moisture variability on the atmosphere, further research is required, particularly on soil moisture-precipitation coupling because soil moisture can influence precipitation by affecting cloud cover via evapotranspiration, leading to the amplification and prolongation of floods and droughts [*Oglesby and Erickson*, 1989 ; *Beljaars et al.*, 1996 ; *Betts*, 2004]. Additionally, both the strength and underlying mechanisms of soil moisture-temperature coupling are model-dependent [*Koster et al.*, 2006]. The contribution of surface albedo variability to soil moisture-temperature coupling, for instance, was important in CRCM5 but quite insignificant in other studies involving other RCMs [*Pal and Eltahir*, 2001 ; *Tawfik and Steiner*, 2011]. Furthermore, the use of different lateral boundary conditions and land surface schemes could lead to even more differences in coupling. As results vary from model to model, it is important to perform model intercomparison studies to improve our understanding of the complex mechanisms of land-atmosphere-coupling.

Acknowledgments : This research was carried out within the framework of the Canadian Network for Regional Climate and Weather Processes (CNRCWP) funded by the Natural Sciences and Engineering Research Council (NSERC). The ERA-40 and ERA-Interim reanalysis data used to drive CRCM5 were obtained from the European Centre for Medium-Range Weather Forecasts (ECMWF). The second-generation Canadian Earth System Model (CanESM2) used to drive CRCM5 is part of the Coupled Model Intercomparison Project (CMIP5).

FIGURES

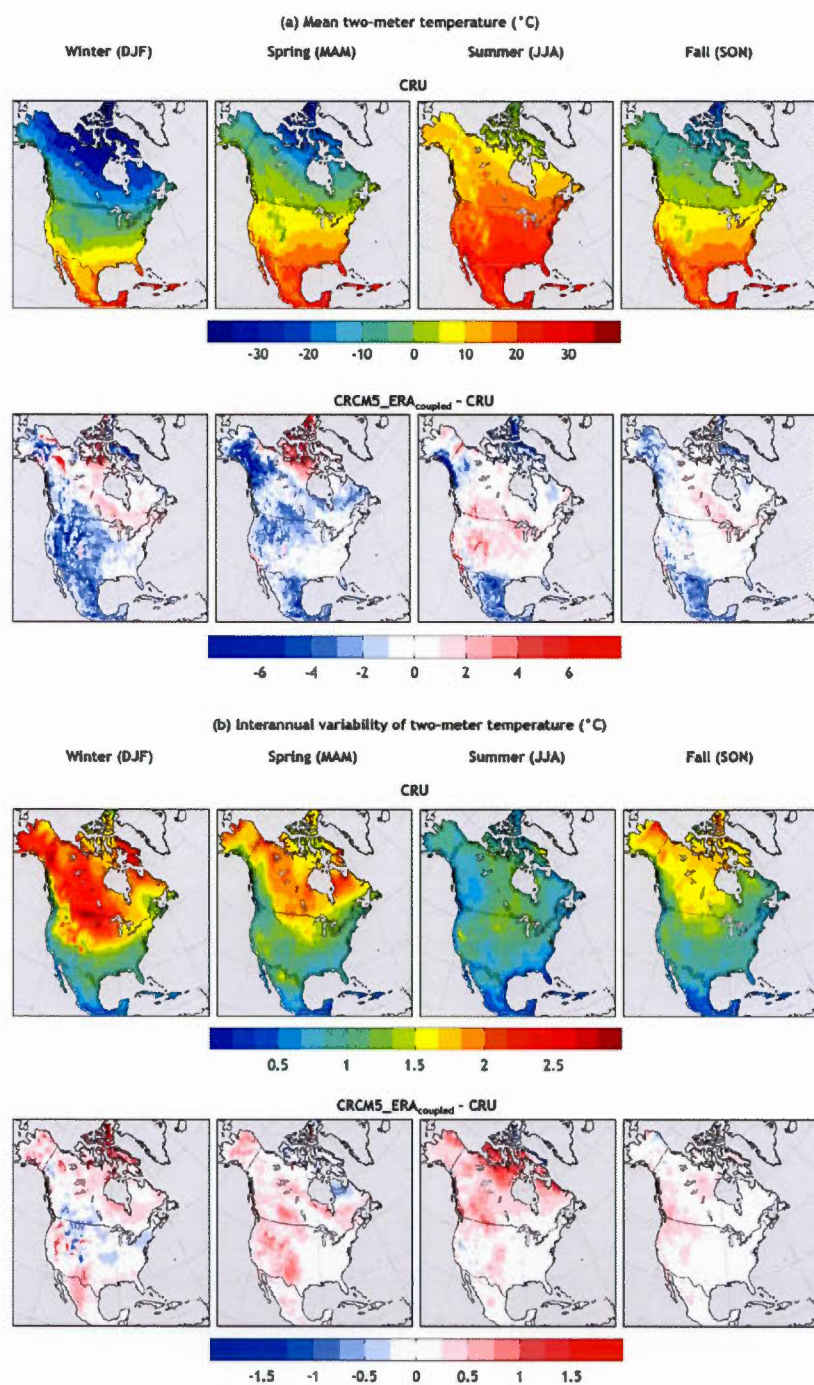


Figure 2.1 (a) Observed (CRU) mean seasonal two-meter temperatures and (b) their interannual variability ($^{\circ}\text{C}$) (top panels) and differences between the CRCM5 simulation driven by ERA Reanalyses and CRU ($\text{CRCM5} - \text{ERA}_{\text{coupled}} - \text{CRU}$) (bottom panels).

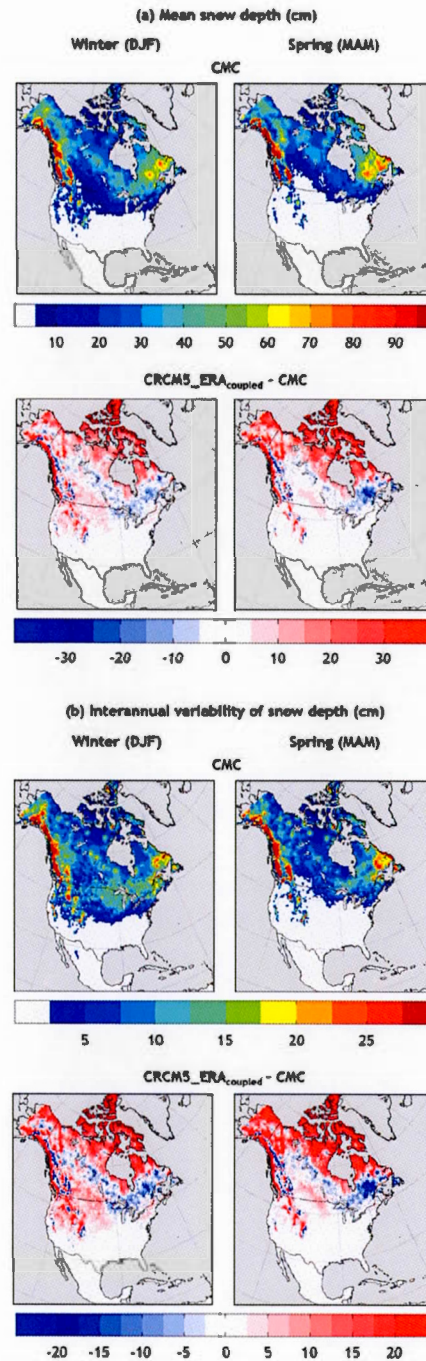


Figure 2.2 (a) Observed (CMC) mean seasonal snow depths and (b) their interannual variability (cm) (top panels) and differences between the CRCM5 simulation driven by ERA Reanalyses and CMC ($\text{CRCM5} - \text{ERA}_{\text{coupled}} - \text{CMC}$) (bottom panels).

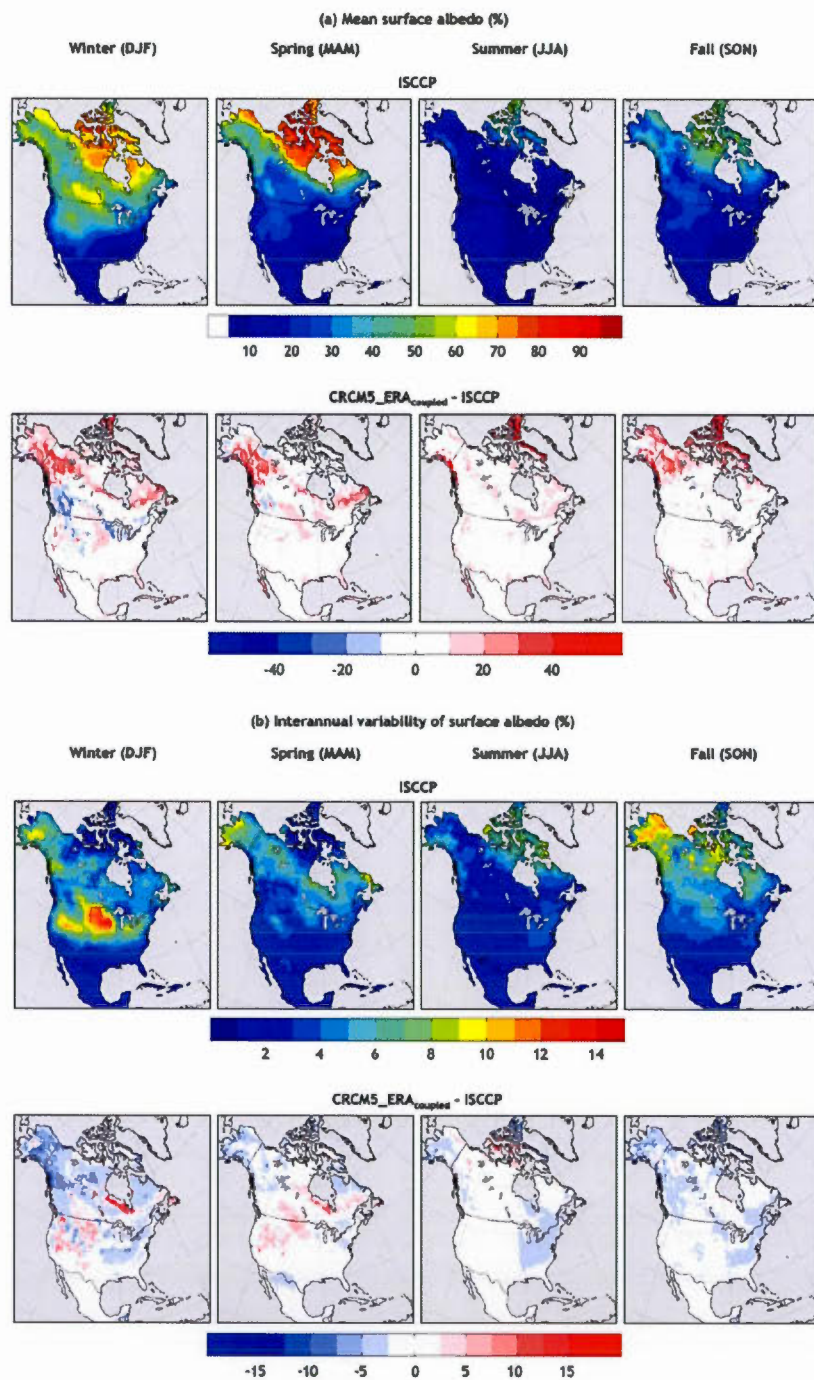


Figure 2.3 (a) Observed (ISCCP) mean seasonal surface albedos and (b) their interannual variability (%) (top panels) and differences between the CRCM5 simulation driven by ERA Reanalyses and ISCCP ($\text{CRCM5} - \text{ERA}_{\text{coupled}} - \text{ISCCP}$) (bottom panels).

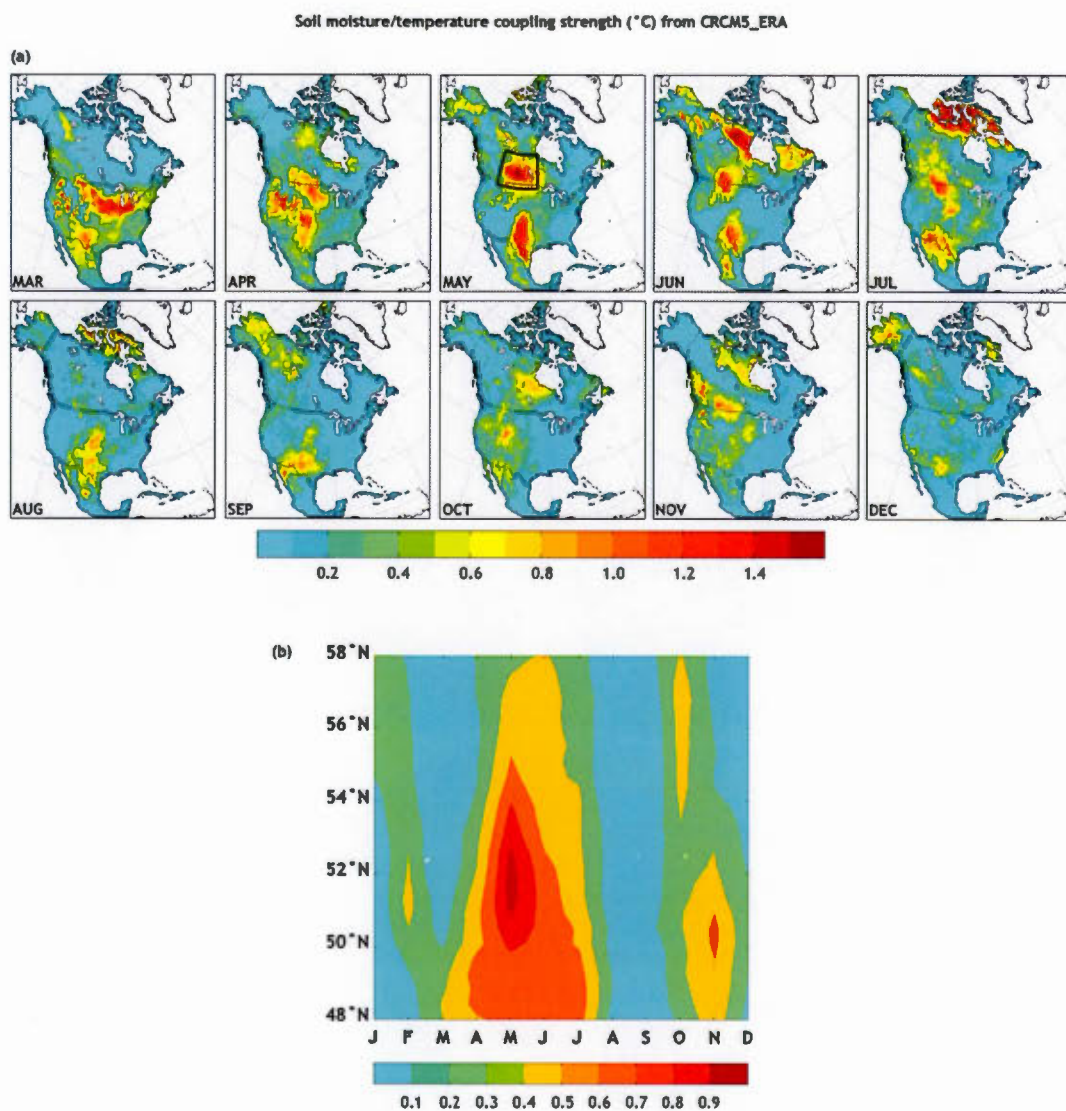


Figure 2.4 (a) Soil moisture-temperature coupling strength ($^{\circ}\text{C}$) ($\Delta\sigma = \sigma_{T,coupled} - \sigma_{T,uncoupled}$) over North America from the ERA-driven CRCM5 simulation for the 1981–2010 period (CRCM5 – ERA) for the March to December period, and (b) zonally averaged monthly soil moisture-temperature coupling strength from CRCM5 – ERA, for the region enclosed by 115°W – 95°W and 48°N – 58°N shown in the middle top panel.

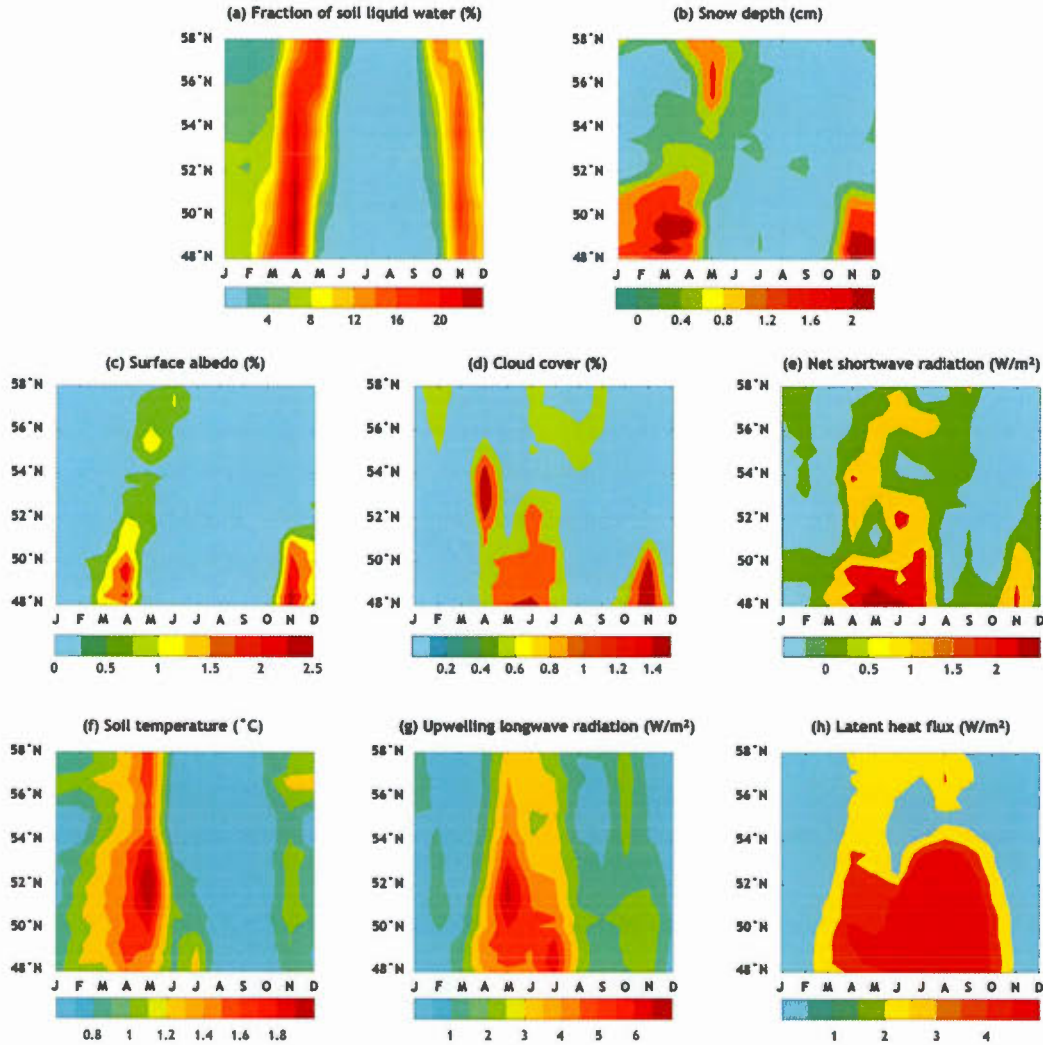


Figure 2.5 (a) Interannual variability of the fraction of soil liquid water for the coupled ERA-driven CRCM5 simulation ($\text{CRCM5} - \text{ERA}_{\text{coupled}}$), and differences in interannual variability between coupled and uncoupled ERA-driven CRCM5 simulations ($\text{CRCM5} - \text{ERA}$) ($\Delta\sigma = \sigma_{\text{coupled}} - \sigma_{\text{uncoupled}}$) averaged over 115°W – 95°W for (b) snow depth (cm), (c) surface albedo (%), (d) cloud cover (%), (e) net shortwave radiation (W/m^2), (f) soil temperature ($^{\circ}\text{C}$), (g) upwelling longwave radiation (W/m^2), and (h) latent heat flux (W/m^2).

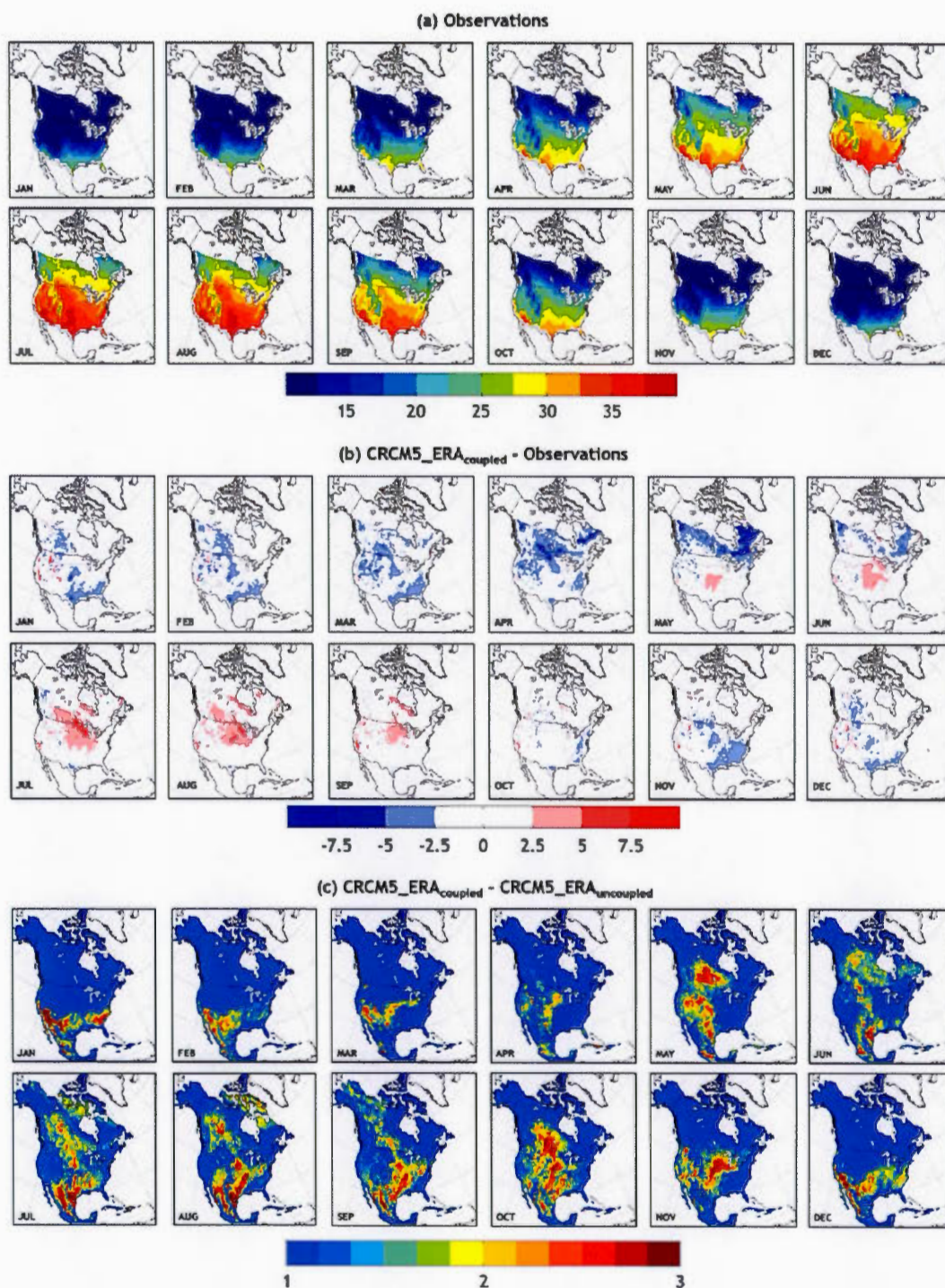


Figure 2.6 (a) 90th percentile of daily maximum temperature ($^{\circ}\text{C}$) from observations, (b) differences between the 90th percentile of maximum temperature ($^{\circ}\text{C}$) from coupled CRCM5 simulations (CRCM5 - ERA_{coupled}) and that from observations, and (c) differences in the mean number of hot days between coupled and uncoupled ERA-driven CRCM5 simulations (CRCM5 - ERA_{coupled} - CRCM5 - ERA_{uncoupled}) for the 1981–2010 period.

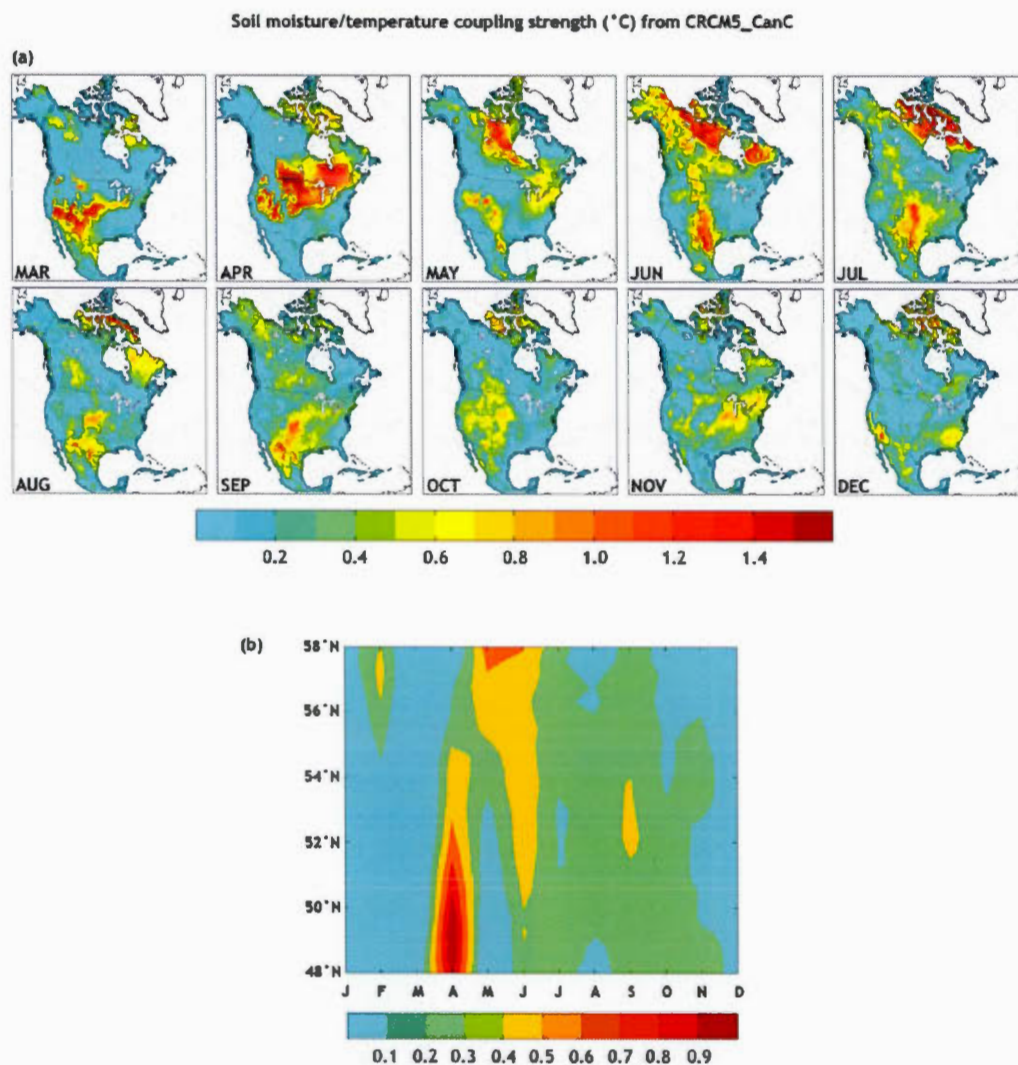


Figure 2.7 As in Figure 2.4, but for the CanESM2-driven CRCM5 simulation performed for the 1981–2010 period (CRCM5 – CanC).

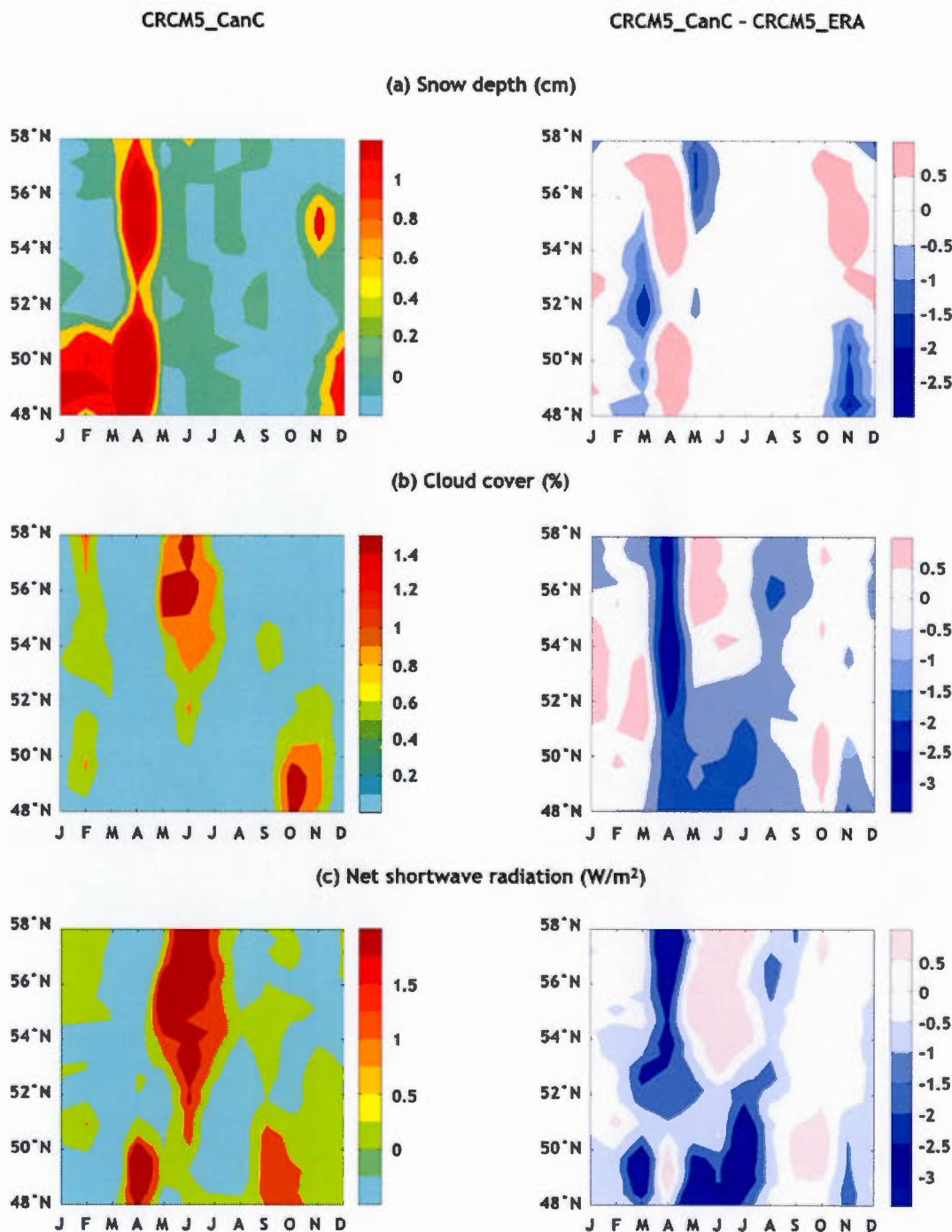


Figure 2.8 Differences in interannual variability between coupled and uncoupled simulations ($\Delta\sigma = \sigma_{\text{coupled}} - \sigma_{\text{uncoupled}}$) for (a) snow depth (cm), (b) cloud cover (%) and (c) net shortwave radiation (W/m^2) for CanESM2-driven CRCM5 simulations (CRCM5 – CanC) (left), and the comparison between CanESM2-driven and ERA-driven CRCM5 simulations (CRCM5 – CanC - CRCM5 – ERA) (right).

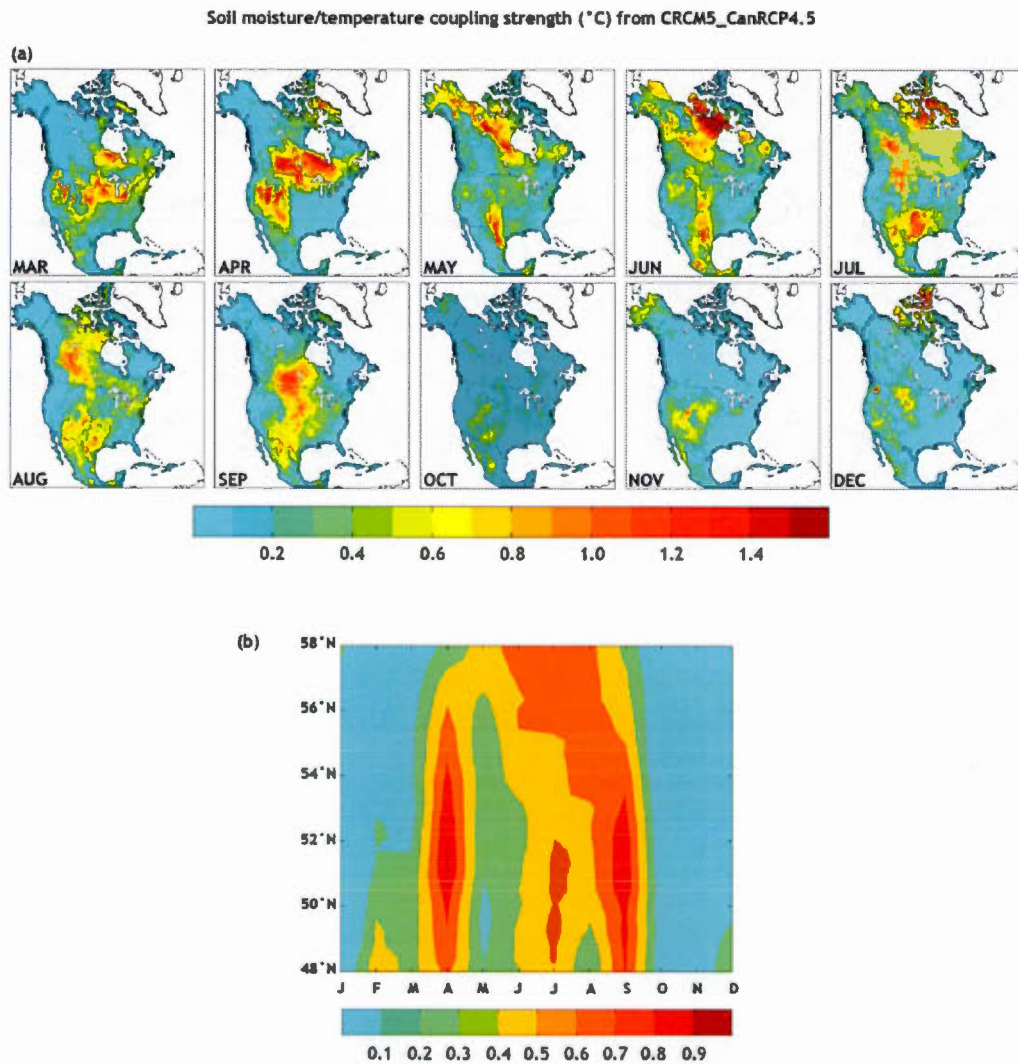


Figure 2.9 As in Figure 2.4, but for the CanESM2-driven CRCM5 simulation performed for the 2071–2100 period for the RCP 4.5 scenario (CRCM5 – CanRCP4.5).

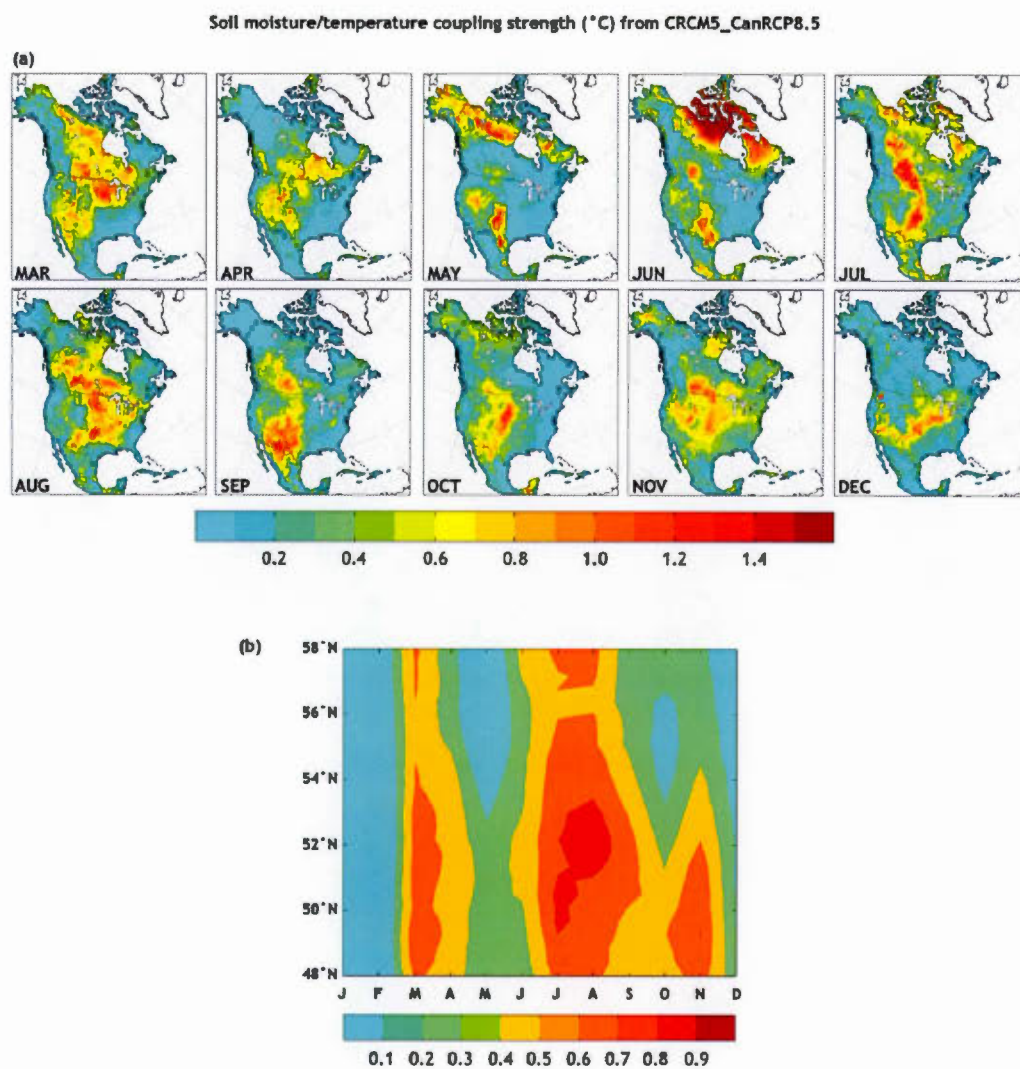


Figure 2.10 As in Figure 2.4, but for the CanESM2-driven CRCM5 simulation performed for the 2071–2100 period for the RCP 8.5 scenario (CRCM5 – CanRCP8.5).

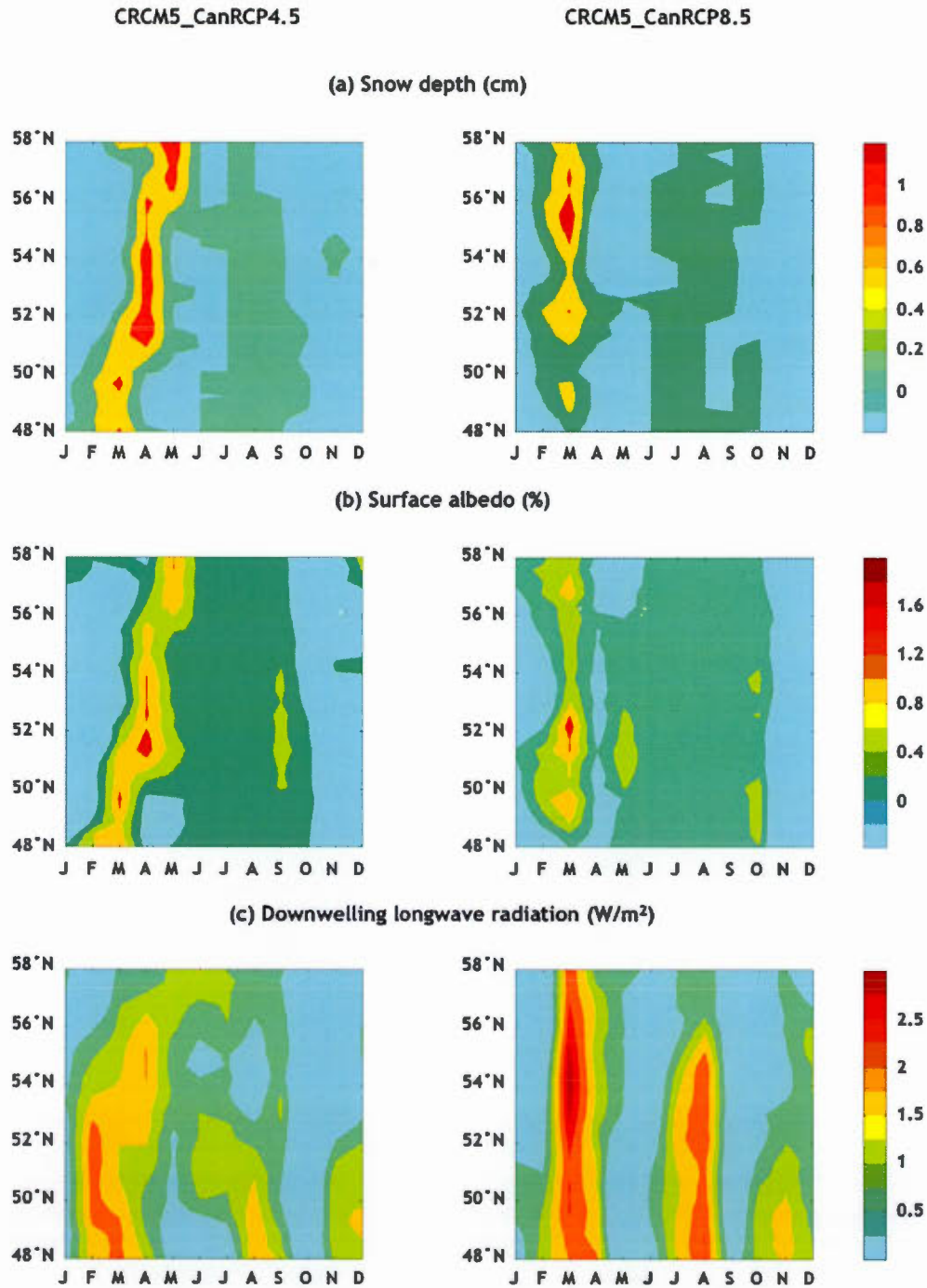


Figure 2.11 Differences in interannual variability between coupled and uncoupled CanESM2-driven CRCM5 simulations ($\Delta\sigma = \sigma_{coupled} - \sigma_{uncoupled}$) for the 2071–2100 period for RCPs 4.5 (left) and 8.5 (right) for (a) snow depth (cm), (b) surface albedo (%), and (c) downwelling longwave radiation (W/m²).

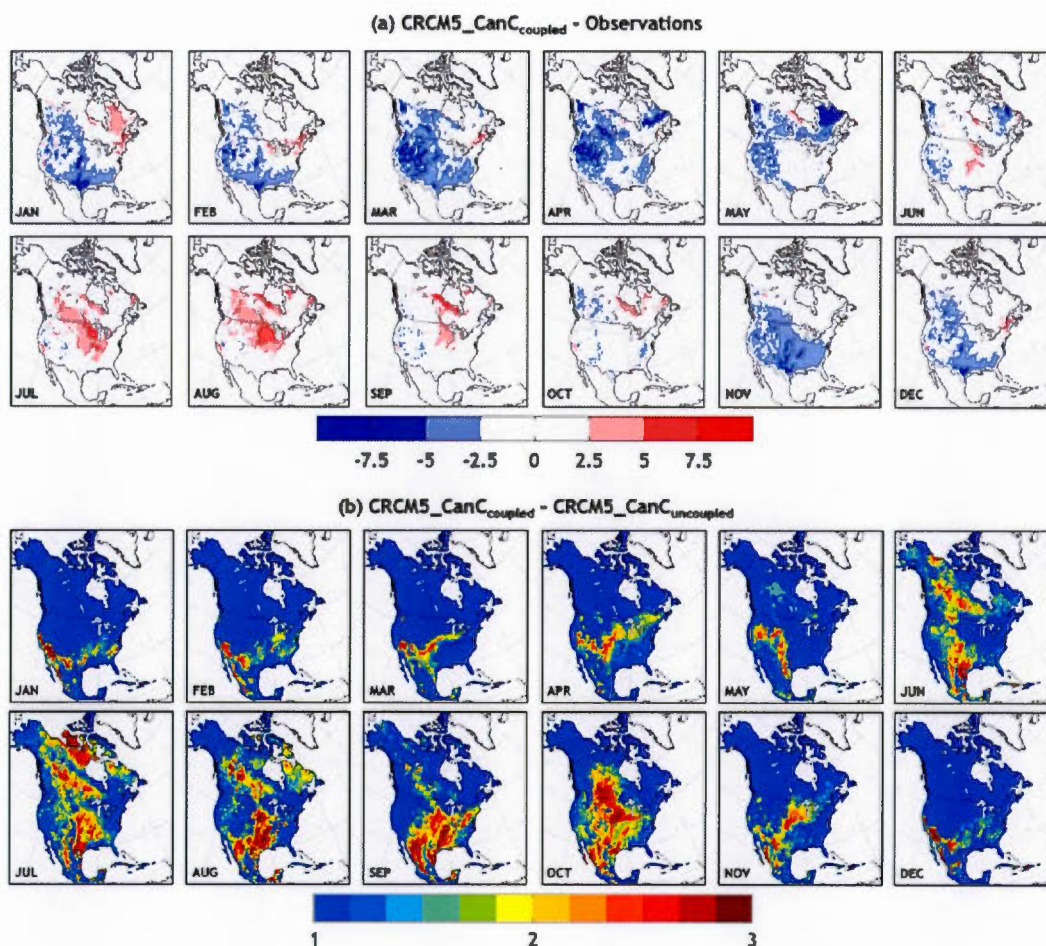


Figure 2.12 (a) Differences between the 90th percentile of maximum temperature ($^{\circ}\text{C}$) obtained from CanESM2-driven CRCM5 simulations ($\text{CRCM5} - \text{CanC}$) and that from observations, and (b) differences in the mean number of hot days between coupled and uncoupled CanESM2-driven CRCM5 simulations ($\text{CRCM5} - \text{CanC}_{\text{coupled}} - \text{CRCM5} - \text{CanC}_{\text{uncoupled}}$) for the 1981–2010 period.

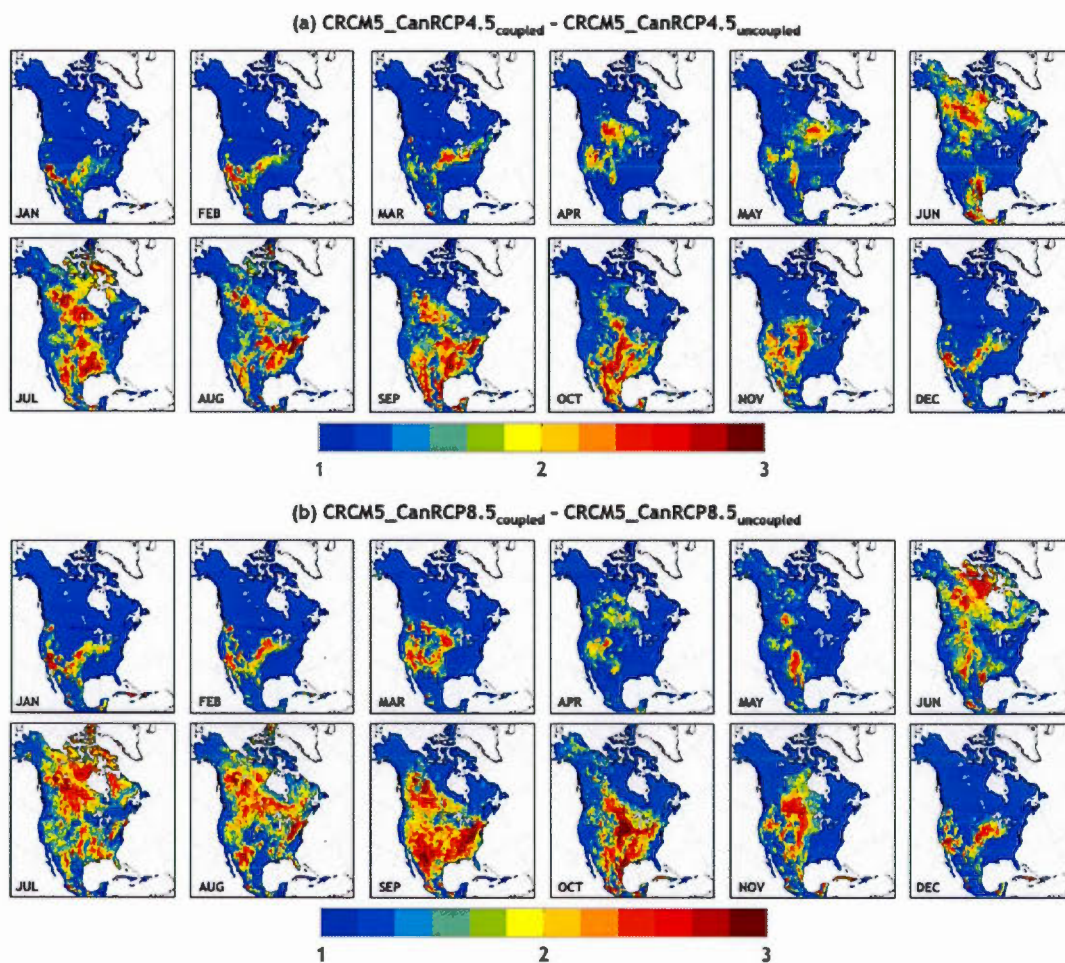


Figure 2.13 Differences in the mean number of hot days between coupled and uncoupled CanESM2-driven CRCM5 simulations for the 2071–2100 period for the (a) RCP 4.5 ($\text{CRCM5} - \text{CanRCP4.5}_{\text{coupled}} - \text{CRCM5} - \text{CanRCP4.5}_{\text{uncoupled}}$) and (b) RCP 8.5 ($\text{CRCM5} - \text{CanRCP8.5}_{\text{coupled}} - \text{CRCM5} - \text{CanRCP8.5}_{\text{uncoupled}}$) scenarios.

TABLES

Table 2.1 List of experiments considered in this study

Experiment	Soil moisture	Time period	Driving data
CRCM5 – ERA _{coupled}	Interactive	1981–2010	ERA-40/ERA-Interim Reanalysis
CRCM5 – ERA _{uncoupled}	Prescribed	1981–2010	ERA-40/ERA-Interim Reanalysis
CRCM5 – CanC _{coupled}	Interactive	1981–2010	CanESM2
CRCM5 – CanC _{uncoupled}	Prescribed	1981–2010	CanESM2
CRCM5 – CanRCP4.5 _{coupled}	Interactive	2071–2100	CanESM2 (RCP 4.5)
CRCM5 – CanRCP4.5 _{uncoupled}	Prescribed	2071–2100	CanESM2 (RCP 4.5)
CRCM5 – CanRCP8.5 _{coupled}	Interactive	2071–2100	CanESM2 (RCP 8.5)
CRCM5 – CanRCP8.5 _{uncoupled}	Prescribed	2071–2100	CanESM2 (RCP 8.5)

CHAPITRE III

CONCLUSION

L'objectif de ce mémoire était d'étudier les différences saisonnières dans l'intensité et les mécanismes du couplage entre l'humidité du sol et la température de l'air en Amérique du Nord à l'aide de simulations couplées et non-couplées, réalisées avec le modèle régional du climat, MRCC5, pour les climats actuel et futur. Dans la simulation couplée, la variabilité interannuelle de l'humidité du sol varie selon le schéma de surface. Mais dans la simulation non-couplée, l'interaction entre l'humidité du sol et la température de l'air est affectée car les contenus en eau liquide et en glace du sol sont remplacés par des moyennes climatologiques à chaque pas de temps. Comme cette modification isole l'effet de la variabilité interannuelle de l'humidité du sol, la différence entre les simulations couplées et non-couplées nous permet de trouver l'intensité du couplage entre l'humidité du sol et la température de l'air.

Comparé aux observations, MRCC5 est capable de représenter la distribution spatiale des moyennes saisonnières et de la variabilité interannuelle de la température de l'air, la profondeur de la neige et l'albédo de surface, qui sont des variables importantes pour comprendre les mécanismes du couplage. Ce résultat nous a donc permis de savoir que MRCC5 était un modèle adéquat pour étudier les différents aspects du couplage. Toutefois, l'humidité du sol, qui est une variable très importante dans l'étude du couplage, n'a pas pu être validée dû au manque de données d'observations. Comme plusieurs

organismes effectuent actuellement des campagnes de mesures pour populer les bases de données d'humidité du sol, cette contrainte ne devrait plus exister dans de futures recherches sur le sujet [Xia *et al.*, 2015].

L'intensité du couplage, qui est calculée en terme de différence de variabilité interannuelle de la température de l'air entre les simulations couplées et non-couplées, a, dans un premier temps, été analysée dans des simulations réalisées avec MRCC5, piloté par les réanalyses ERA-Interim, pour le climat actuel. Nos résultats indiquent qu'il y a d'importantes différences saisonnières dans les mécanismes et l'intensité du couplage. Dans MRCC5, le couplage évolue différemment au sud et au nord de la région qui s'étend du sud des Grandes Plaines au sud des Prairies Canadiennes. Au sud, le couplage reste au même endroit à l'année longue mais son intensité évolue pendant l'année et atteint un pic en été. Pal et Eltahir [2001] ainsi que Seneviratne *et al.* [2010] ont démontré que le couplage est fort en été car l'humidité du sol influence la répartition du rayonnement net dans les flux de chaleur latente et sensible. Le flux de chaleur latente, en particulier, est un indicateur du taux d'évapotranspiration. Vu que l'évapotranspiration refroidit l'air, elle agit comme un processus intermédiaire dans la rétroaction entre l'humidité du sol et la température de l'air.

Au nord, plus particulièrement la région qui recouvre le sud des Prairies Canadiennes, le couplage n'est pas fixe mais évolue géographiquement pendant l'année. L'intensité maximale du couplage migre vers le nord au printemps et vers le sud en automne. Ceci démontre que l'état de l'eau dans le sol (contenu en eau liquide vs contenu en glace du sol) est un mécanisme important à considérer. Pour trouver les autres mécanismes du couplage, nous avons ensuite calculé la différence entre les simulations couplées et non-couplées pour d'autres variables potentiellement influencées par l'absence de variabilité interannuelle de l'humidité du sol dans les simulations non-couplées.

Cette analyse a démontré que l'état de l'eau dans le sol et la profondeur de la neige

influencent tous les deux l'albédo de surface. Comme l'albédo de surface est tout simplement le rapport entre le rayonnement court sortant et entrant, celui-ci affecte le rayonnement net à la surface. Selon le bilan d'énergie à la surface, la quantité de rayonnement court absorbé se reflète dans la température du sol et dans la quantité de rayonnement long sortant. Ainsi, le rayonnement net à la surface influence les flux sortant. Au printemps et en automne, le rayonnement long sortant, en particulier, semble être responsable de la plus grande variabilité de température observée dans les simulations couplées. Le flux de chaleur latente, indicateur du taux d'évapotranspiration, quant à lui, joue un rôle moins important au printemps qu'en été. Par un effet de rétroaction, la température de l'air influence ensuite de nouveau la profondeur de la neige, qui influence à son tour l'albédo de surface. La figure A4 résume ces mécanismes du couplage hypothétiques pour le printemps et l'automne.

Comme il est surtout important d'étudier le couplage pour savoir comment l'humidité du sol peut amplifier et prolonger les conditions extrêmes, l'une de nos analyses consistait à connaître l'effet de la variabilité de l'humidité du sol sur le nombre de journées chaudes, qui sont définies comme étant des journées où la température maximale journalière dépasse le 90^e centile. Nos résultats indiquent que l'humidité du sol amplifie bel et bien le nombre de journées chaudes au mois de mai, surtout sur la partie sud des Prairies Canadiennes, là où le couplage entre l'humidité du sol et la température de l'air est également fort. Cette région des Prairies Canadiennes est grandement utilisée pour l'agriculture. Pour des raisons économiques, il est donc important de mieux pouvoir prédire les phénomènes météorologiques extrêmes sur cette région. Pour se rapprocher de ce but, les mécanismes du couplage doivent alors être mieux représentés dans les modèles de prévision numériques.

La dernière partie de l'étude était dédiée à connaître les changements futurs dans le couplage sous l'effet du réchauffement climatique. Pour ce faire, nous avons utilisé des simulations réalisées avec MRCC5, piloté par le modèle global, CanESM2. Des scénar-

rios représentatifs de concentrations de gaz à effet de serre (les RCPs 4,5 et 8,5) ont été utilisés pour représenter le climat futur. Nous avons tout d'abord démontré que l'utilisation de différentes conditions aux frontières latérales pouvait engendrer des différences importantes entre les simulations. Dans le climat actuel, la plus grosse différence était l'absence d'un fort couplage en mai et en novembre sur le sud des Prairies Canadiennes dans les simulations MRCC5, piloté par CanESM2. Des analyses plus poussées ont permis de démontrer que ceci était le résultat d'une plus basse profondeur de la neige et d'une plus faible couverture nuageuse dans ces simulations comparées à celles qui ont été réalisées avec le même modèle, piloté par les réanalyses ERA-Interim. Contrairement à la profondeur de la neige, la couverture nuageuse n'avait pas été identifiée comme étant un mécanisme important du couplage au préalable. L'humidité du sol, elle-même, peut influencer la couverture nuageuse en affectant l'évapotranspiration, qui contribue ensuite à la convection. La couverture nuageuse, quant à elle, influence l'albédo planétaire, qui, comme l'albédo de surface, est relié au rayonnement net à la surface. Comme mentionné plus tôt, cette relation entre une grande variabilité de l'albédo et une grande variabilité du rayonnement net finit par se traduire par une plus grande variabilité dans la température de l'air. La plus faible couverture nuageuse dans les simulations MRCC5, piloté par CanESM2, contribue alors à un faible couplage en mai et en novembre.

Malgré ces différences, l'intensité et les mécanismes du couplage pendant le printemps (la saison de fonte de la neige) sont similaires dans les deux simulations. Cette similarité notable nous a donc poussé à poursuivre l'analyse pour le climat futur. Les changements observés pour le climat futur comparé au climat présent sont surtout reliés à des différences dans trois éléments du mécanisme du couplage. Premièrement, dans les deux scénarios utilisés, un couplage plus conséquent est observé en été sur le sud des Prairies Canadiennes. L'humidité du sol à cet endroit est moins élevée dans le futur en raison d'une plus faible précipitation. En conséquence, l'évapotranspiration est limitée

par l'humidité du sol et le couplage est fort car la rétroaction entre humidité du sol et la température de l'air est plus importante. Dans le scénario RCP 8,5, qui représente une augmentation de concentration de gaz à effet de serre plus marquante, des changements importants dans deux autres éléments du mécanisme du couplage sont observés. Tout d'abord, comme la période de la fonte de la neige débute plus tôt comparé au climat présent, l'effet de la variabilité de la neige sur l'albédo de surface est également visible plus tôt dans l'année. Ceci mène à plus de variabilité dans la température et un fort couplage prématuré. De plus, l'effet du rayonnement long entrant sur la température de l'air est plus marquante. Ceci est dû à une plus grande couverture nuageuse, amplifiée par une concentration de gaz à effet de serre plus élevée, qui mène à de plus fortes émissions de rayonnement infrarouge vers le sol.

L'influence de la variabilité de l'humidité du sol sur les températures extrêmes pour le climat futur a également été estimée de la même façon que pour le climat présent. Ainsi, nous avons observé que le nombre de journées chaudes est plus élevé dans les simulations couplées que dans les simulations non-couplées. De plus, l'influence de la variabilité de l'humidité du sol sur les températures extrêmes s'étend sur une plus grande zone géographiquement. Dans le climat présent, cette influence est conséquente surtout pour la région des Grandes Plaines et des Prairies Canadiennes, mais dans le climat futur, elle est aussi importante pour les côtes est et ouest des États-Unis et les régions nordiques du Canada. Ceci est probablement lié au fait que les sols plus secs pour ces régions dans le futur mènent à un plus fort couplage, menant à un effet de rétroaction plus important entre l'humidité du sol et la température de l'air.

Même si ce mémoire touche plusieurs aspects du couplage, il n'est pas pour autant exhaustif. Tout d'abord, l'influence de l'humidité du sol sur l'atmosphère ne s'arrête pas à la température. Plusieurs études ont en effet démontré que l'humidité du sol pouvait aussi affecter la précipitation [Oglesby et Erickson, 1989 ; Beljaars et al., 1996] et mener à l'amplification et la prolongation d'inondations et de sécheresses. Le couplage entre

l'humidité du sol et la précipitation pourrait donc faire l'objet d'une autre étude dans le futur. Cependant, ce genre d'étude pourrait engendrer un bon nombre de difficultés car les mécanismes du couplage entre l'humidité du sol et la précipitation sont beaucoup plus complexes que ceux du couplage entre l'humidité du sol et la température [Lawrence et Slingo, 2005 ; Seneviratne et al., 2010 ; Diro et al., 2014].

De plus, plusieurs études précédentes n'ont pas attribué de rôle significatif à l'albédo de surface dans le couplage pendant l'été, le printemps et l'automne [Pal et Eltahir, 2001 ; Tawfik et Steiner, 2011]. Ceci peut être dû au fait que chaque étude utilise un modèle différent, couplé avec un schéma de surface différent et possédant des paramètres physiques et des conditions aux frontières latérales distincts. Pour approfondir nos connaissances sur le couplage, il est donc important de faire des études de comparaison de modèles.

ANNEXE A

FIGURES COMPLÉMENTAIRES

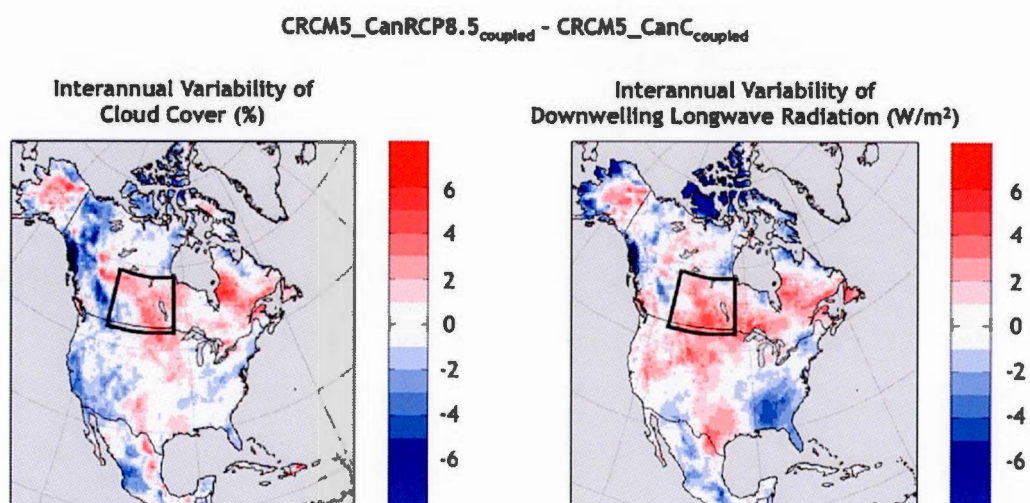


Figure A1. Differences between $\text{CRCM5_CanRCP8.5}_{\text{coupled}}$ and $\text{CRCM5_CanC}_{\text{coupled}}$ simulated (a) interannual variability of cloud cover (%), and (b) interannual variability of downwelling longwave radiation (W/m^2) for November.

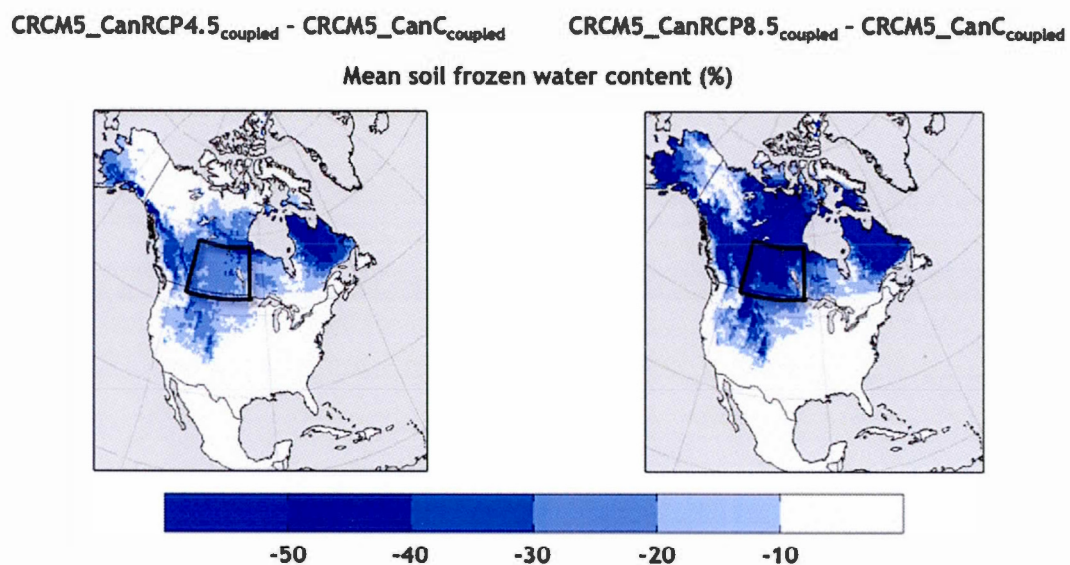


Figure A2. Differences between $\text{CRCM5_CanRCP4.5}_{\text{coupled}}$ and $\text{CRCM5_CanC}_{\text{coupled}}$ (left), and $\text{CRCM5_CanRCP8.5}_{\text{coupled}}$ and $\text{CRCM5_CanC}_{\text{coupled}}$ (right) for the mean soil frozen water content (%) in the top 10-cm soil layer for November.

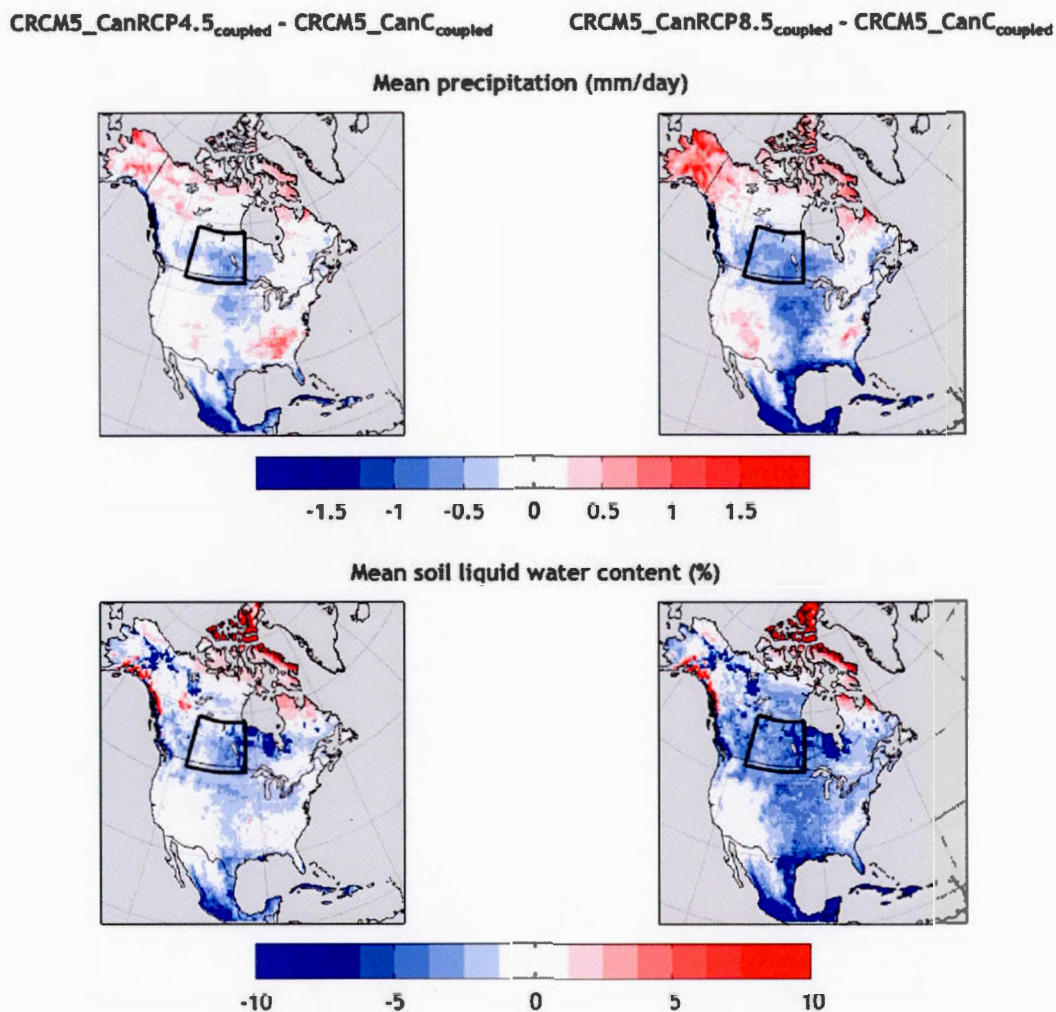


Figure A3. Differences between CRCM5_CanRCP4.5_{coupled} and CRCM5_CanC_{coupled} (left), and CRCM5_CanRCP8.5_{coupled} and CRCM5_CanC_{coupled} (right) for the mean precipitation (mm/day) (top panels) and mean soil liquid water content (%) in the top 10-cm soil layer for the summer season.

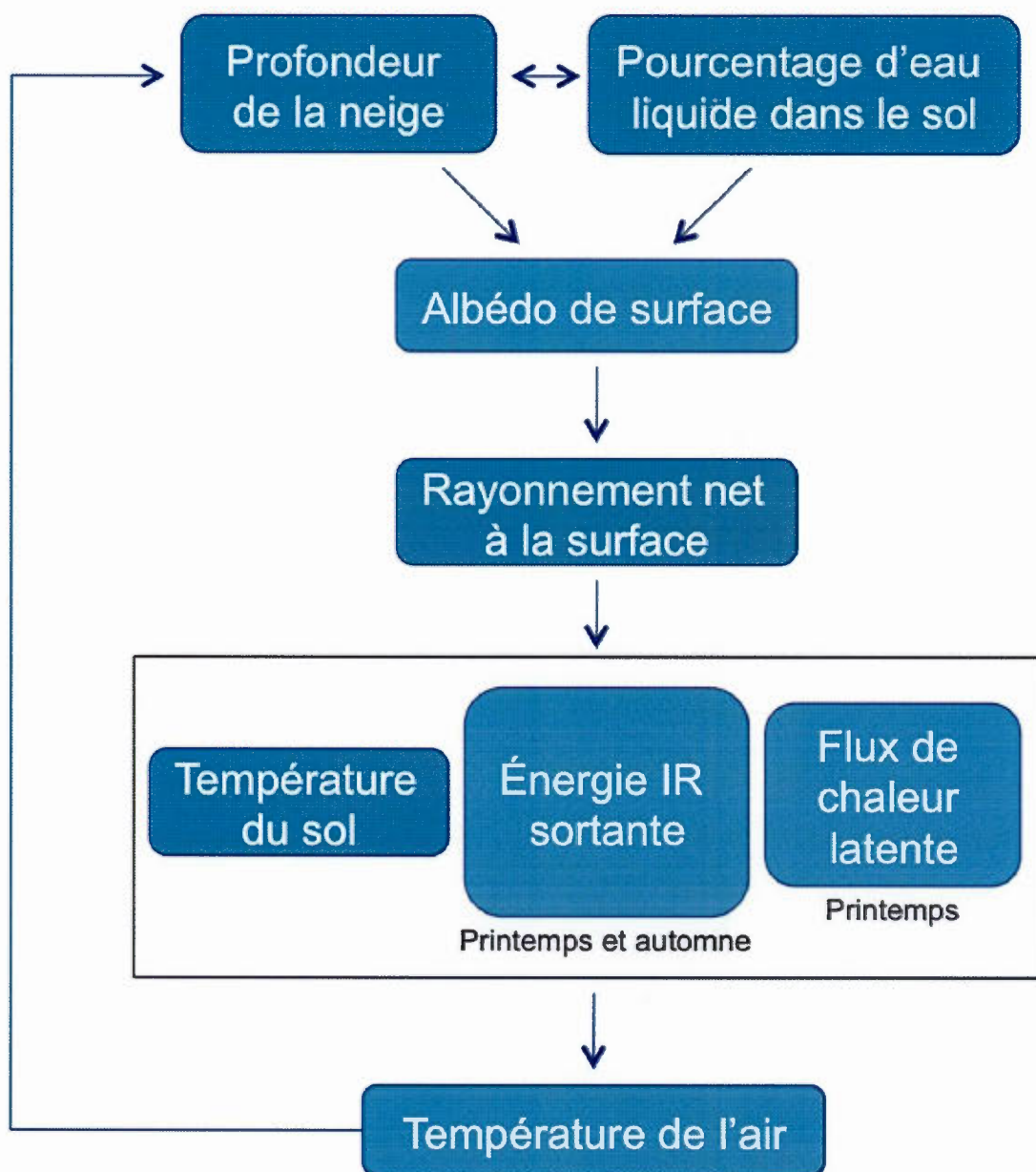


Figure A4. Schéma montrant les corrélations hypothétiques entre le pourcentage d'eau liquide dans le sol, la profondeur de la neige, l'albédo de surface, le rayonnement net à la surface, la température du sol, l'énergie infrarouge sortante, le flux de chaleur latente, et la température de l'air.

RÉFÉRENCES

- Arora, V. K., Scinocca, J. F., Boer, G. J., Christian, J. R., Denman, K. L., Flato, G. M., Kharin, V. V., Lee, W. G., and Merryfield, W. J. (2011). Carbon emission limits required to satisfy future representative concentration pathways of greenhouse gases. *Geophysical Research Letters* 38, L05805, doi :10.1029/2010GL046270.
- Bartlett, P. A., and Verseghy, D. L. (2015). Modified treatment of intercepted snow improves the simulated forest albedo in the Canadian Land Surface Scheme. *Hydrological Processes* 29, 3208-3226.
- Bélair, S., Mailhot, J., Girard, C., and Vaillancourt, P. (2005). Boundary layer and shallow cumulus clouds in a medium-range forecast of a large-scale weather system. *Monthly Weather Review* 133, 1938–1960.
- Beljaars, A. C., Viterbo, P., Miller, M. J., and Betts, A. K. (1996). The anomalous rainfall over the United States during July 1993 : Sensitivity to land surface parameterization and soil moisture anomalies. *Monthly Weather Review* 124, 362–383.
- Benoit, R., Côté, J., and Mailhot, J. (1989). Inclusion of a TKE boundary layer parameterization in the Canadian regional finite-element model. *Monthly Weather Review* 117, 1726–1750.
- Betts, A. K. (2004). Understanding hydrometeorology using global models. *Bulletin of the American Meteorological Society* 85, 1673–1688.
- Bradshaw, B., Dolan, H., and Smit, B. (2004). Farm-level adaptation to climatic variability and change : crop diversification in the Canadian prairies. *Climatic Change* 67, 119–141.

- Brown, R. D., Brasnett, B., and Robinson, D. (2003). Gridded North American monthly snow depth and snow water equivalent for GCM evaluation. *Atmosphere-Ocean* 41, 1–14.
- Cohen, S., and Miller, K. (2001). 'North America', in McCarthy, J. J., Canziani, O. F., Learty, N. A., Dokken, D. J., and White, K. S. (eds.), *Climate Change 2001 : Impacts, Adaptation and Vulnerability*, Intergovernmental Panel on Climate Change, Geneva. Cambridge University Press, Cambridge, U.K. and New York, U.S.A., 735–800.
- Côté, J., Gravel, S., Méthot, A., Patoine, A., Roch, M., and Staniforth, A. (1998) The Operational CMC-MRB Global Environmental Multiscale (GEM) Model. Part I : design considerations and formulation. *Monthly Weather Review* 126, 1373–1395
- Dee, D. P., Uppala, S. M., Simmons, A. J., Berrisford, P., Poli, P., Kobayashi, S., Andrae, U., Balmaseda, M. A., Balsamo, G., Bauer, P., Bechtold, P., Beljaars, A. C. M., van de Berg, L., Bidlot, J., Bormann, N., Delsol, C., Dragani, R., Fuentes, M., Geer, A. J., Haimberger, L., Healy, S. B., Hersbach, H., Hólm, E. V., Isaksen, L., Kållberg, P., Köhler, M., Matricardi, M., McNally, A. P., Monge-Sanz, B. M., Morcrette, J.-J., Park, B.-K., Peubey, C., de Rosnay, P., Tavolato, C., Thépaut, J.-N., and Vitart, F. (2011). The ERA-Interim reanalysis : Configuration and performance of the data assimilation system. *Quarterly Journal of the Royal Meteorological Society* 137, 553–597.
- Delage, Y. (1997). Parameterising sub-grid scale vertical transport in atmospheric models under statically stable conditions. *Boundary-Layer Meteorology* 82, 23–48.
- Delage, Y., and Girard, C. (1992). Stability functions correct at the free convection limit and consistent for both the surface and Ekman layers. *Boundary-Layer Meteorology* 58, 19–31.
- Diro, G. T., Sushama, L., Martynov, A., Jeong, D. I., Versegny, D., and Winger, K.

- (2014). Land-atmosphere coupling over North America in CRCM5. *Journal of Geophysical Research : Atmospheres* 119, 11955–11972.
- Diro, G. T., and Sushama, L. (2016). The role of land-atmosphere interaction on future hot spells over North America as simulated by the Canadian Regional Climate Model (CRCM5). Submitted to *Journal of Climate*.
- Fischer, E. M., Seneviratne, S. I., Lüthi, D., and Schär, C. (2007). Contribution of land-atmosphere coupling to recent European summer heat waves. *Geophysical Research Letters* 34, doi : 10.1029/2006GL029068.
- Fischer, E. M., Seneviratne, S. I., Vidale, P. L., Lüthi, D., and Schär, C. (2007). Soil moisture-atmosphere interactions during the 2003 European summer heat wave. *Journal of Climate* 20, 5081–5099.
- Giorgi, F., Coppola, E., Solomon, F., Mariotti, L., Sylla, M. B., Bi, X., Elguindi N, Diro, G. T., Nair, V., Giuliani, G., and Turuncoglu, U. U. (2012). RegCM4 : model description and preliminary tests over multiple CORDEX domains. *Climate Research* 52, 7–29.
- Herrington, R., Johnson, B., and Hunter, F. (1997). Responding to global climate change in the Prairies. Canada Country Study : Climate Impacts and Adaptations, Vol. III, Environment Canada, Ottawa.
- Harris, I., Jones, P. D., Osborn, T. J., and Lister, D. H. (2014). Updated high-resolution grids of monthly climatic observations - the CRU TS3.10 Dataset. *International Journal of Climatology* 34, 623–642.
- Hopkinson, R. F., McKenney, D. W., Milewska, E. J., Hutchinson, M. F., Papadopol, P., and Vincent, L. A. (2011). Impact of aligning climatological day on gridding daily maximum-minimum temperature and precipitation over Canada. *Journal of Applied Meteorology and Climatology* 50, 1654–1665.

- Hutchinson, M. F., McKenney, D. W., Lawrence, K., Pedlar, J. H., Hopkinson, R. F., Milewska, E., and Papadopol, P. (2009). Development and testing of Canada-wide interpolated spatial models of daily minimum-maximum temperature and precipitation for 1961–2003. *Journal of Applied Meteorology and Climatology* 48, 725–741.
- Kain, J. S., and Fritsch, J. M. (1990). A one-dimensional entraining/detraining plume model and its application in convective parameterization. *Journal of the Atmospheric Sciences* 47, 2784–2802.
- Koster, R. D., Dirmeyer, P. A., Guo, Z., Bonan, G., Chan, E., Cox, P., Gordon, C. T., Kanae, S., Kowalczyk, E., Lawrence, D., Liu, P., Lu, C.-H., Malyshev, S., McAvaney, B., Mitchell, K., Mocko, D., Oki, T., Oleson, K., Pitman, A., Sud, Y. C., Taylor, C. M., Verseghy, D., Vasic, R., Xue, Y., and Yamada, T. (2004). Regions of strong coupling between soil moisture and precipitation. *Science* 305, 1138–1140.
- Koster, R. D., Guo, Z., Dirmeyer, P. A., Bonan, G., Chan, E., Cox, P., Davies, H., Gordon, C. T., Kanae, S., Kowalczyk, E., Lawrence, D., Liu, P., Lu, C.-H., Malyshev, S., McAvaney, B., Mitchell, K., Mocko, D., Oki, T., Oleson, K. W., Pitman, A., Sud, Y. C., Taylor, C. M., Verseghy, D., Vasic, R., Xue, Y., and Yamada, T. (2006). GLACE : The Global Land-Atmosphere Coupling Experiment, Part I : Overview. *Journal of Hydrometeorology* 7, 590–610.
- Koster, R. D., Mahanama, S. P. P., Yamada, T. J., Balsamo, G., Berg, A. A., Boisserie, M., Dirmeyer, P. A., Doblas-Reyes, F. J., Drewitt, G., Gordon, C. T., and Guo, Z. (2010). Contribution of land surface initialization to subseasonal forecast skill : First results from a multi-model experiment. *Geophysical Research Letters* 37, L02402, doi :10.1029/2009GL041677.
- Kuo, H. (1965). On formation and intensification of tropical cyclones through latent heat release by cumulus convection. *Journal of Atmospheric Sciences* 22, 40–63.

- Laprise, R. (1992). The Euler equations of motion with hydrostatic pressure as an independent variable. *Monthly Weather Review* 120, 197–207.
- Lawrence, D. M., and Slingo, J. M. (2005). Weak land-atmosphere coupling strength in HadAM3 : The role of soil moisture variability. *Journal of Hydrometeorology* 6, 670–680.
- Li, J., and Barker, H. W. (2005). A radiation algorithm with correlated-k distribution. Part I : Local thermal equilibrium. *Journal of the Atmospheric Sciences* 62, 286–309.
- Luciuk, G., and O'Brien, E. (1999). Adaptation, Agriculture and Water Resources, Prairie Farm Rehabilitation Administration Paper, Agriculture and Agri-Food Canada, Regina.
- Martynov, A., Sushama, L., and Laprise, R. (2010). Simulation of temperate freezing lakes by one-dimensional lake models : performance assessment for interactive coupling with regional climate models. *Boreal Environment Research* 15, 143–164.
- Martynov, A., Sushama, L., Laprise, R., Winger, K., and Dugas, B. (2012). Interactive lakes in the Canadian Regional Climate Model, version 5 : the role of lakes in the regional climate of North America. *Tellus A* 64, 16226–16245.
- Martynov, A., Laprise, R., Sushama, L., Winger, K., Šeparović, L., and Dugas, B. (2013). Reanalysis-driven climate simulation over CORDEX North America domain using the Canadian regional climate model, version 5 : Model performance evaluation, *Climate Dynamics* 41, 2973–3005.
- McFarlane, N. A. (1987). The effect of orographically excited gravity wave drag on the general circulation of the lower stratosphere and troposphere. *Journal of the Atmospheric Sciences* 44, 1775–1800.

- Mei, R., Wang, G., and Gu, H. (2013). Summer land-atmosphere coupling strength over the United States : Results from the regional climate model RegCM4-CLM3. 5. *Journal of Hydrometeorology* 14, 946–962.
- Moss, R., Babiker, M., Brinkman, S., Calvo, E., Carter, T., Edmonds, J., Elgizouli, I., Emori, S., Erda, L., Hibbard, K., Jones, R., Kainuma, M., Kelleher, J., Lamarque, J. F., Manning, M., Matthews, B., Meehl, J., Meyer, L., Mitchell, J., Nakicenovic, N., O'Neill, B., Pichs, R., Riahi, K., Rose, S., Runci, P., Stouffer, R., van Vuuren, D., Weyant, J., Wilbanks, T., van Ypersele, J. P., and Zurek, M. (2008). Towards New Scenarios for Analysis of Emissions, Climate Change, Impacts, and Response Strategies. Geneva : Intergovernmental Panel on Climate Change.
- Oglesby, R. J., and Erickson, D. J. (1989). Soil moisture and the persistence of North American drought. *Journal of Climate* 2, 1362–1380.
- Oleson, K. W., Niu, G. Y., Yang, Z. L., Lawrence, D. M., Thornton, P. E., Lawrence, P. J., Stöckli, R., Dickinson, R. E., Bonan, G. B., Levis, S., and Dai, A. (2008). Improvements to the Community Land Model and their impact on the hydrological cycle. *Journal of Geophysical Research : Biogeosciences* 113(G1).
- Pal, J. S., and Eltahir, E. A. (2001). Pathways relating soil moisture conditions to future summer rainfall within a model of the land-atmosphere system. *Journal of Climate* 14, 1227–1242.
- Pal, J. S., Giorgi, F., Bi, X., Elguindi, N., Solmon, F., Rauscher, S. A., Gao, X., Francisco, R., Zakey, A., Winter, J., and Ashfaq, M. (2007). Regional climate modeling for the developing world : the ICTP RegCM3 and RegCNET. *Bulletin of the American Meteorological Society* 88, 1395–1409.
- Riahi, K., Rao, S., Krey, V., Cho, C., Chirkov, V., Fischer, G., Kindermann, G., Naki-

- cenovic, N., and Rafaj, P. (2011). RCP 8.5 - A scenario of comparatively high greenhouse gas emissions. *Climatic Change* 109, 33–57.
- Rossow, W. B. and Schiffer, R. A. (1999). Advances in understanding clouds from ISCCP. *Bulletin of the American Meteorological Society* 80, 2261–2287.
- Seneviratne, S. I., Lüthi, D., Litschi, M., and Schär, C. (2006). Land-atmosphere coupling and climate change in Europe. *Nature* 443, 205–209.
- Seneviratne, S. I., Corti, T., Davin, E. L., Hirschi, M., Jaeger, E. B., Lehner, I., Orlowsky, B., and Teuling, A. J. (2010). Investigating soil moisture–climate interactions in a changing climate : A review. *Earth-Science Reviews* 99, 125–161.
- Šeparović, L., Alexandru, A., Laprise, R., Martynov, A., Sushama, L., Winger, K., Tete, K., and Valin, M. (2013). Present climate and climate change over North America as simulated by the fifth-generation Canadian regional climate model. *Climate Dynamics* 41, 3167–3201.
- Skamarock, W. C., Klemp, J. B., Dudhia, J., Gill, D. O., Barker, D. M., Wang, W., and Powers, J. G. (2005). A description of the advanced research WRF version 2 (No. NCAR/TN-468+ STR). National Center For Atmospheric Research Boulder Co Mesoscale and Microscale Meteorology Div.
- Sundqvist, H., Berge, E., and Kristjánsson, J. E. (1989). Condensation and cloud parameterization studies with a mesoscale numerical weather prediction model. *Monthly Weather Review* 117, 1641–1657.
- Tawfik, A. B., and Steiner, A. L. (2011). The role of soil ice in land-atmosphere coupling over the United States : A soil moisture-precipitation winter feedback mechanism. *Journal of Geophysical Research* 116, D02113, doi : 10.1029/2010JD014333.
- Uppala, S. M., Kållberg, P. W., Simmons, A. J., Andrae, U., Bechtold, V. D. C., Fiorino, M., Gibson, J. K., Haseler, J., Hernandez, A., Kelly, G. A., Li, X., Onogi, K., Saarinen,

- S., Sokka, N., Allan, R. P., Andersson, E., Arpe, K., Balmaseda, M. A., Beljaars, A. C. M., Berg, L. V. D., Bidlot, J., Bormann, N., Caires, S., Chevallier, F., Dethof, A., Dragosavac, M., Fisher, M., Fuentes, M., Hagemann, S., Hólm, E., Hoskins, B. J., Isaksen, I., Janssen, P. A. E. M., Jenne, R., McNally, A. P., Mahfouf, J.-F., Morcrette, J.-J., Rayner, N. A., Saunders, R. W., Simon, P., Sterl, A., Trenberth, K. E., Untch, A., Vasiljevic, D., Viterbo, P. and Woollen, J. (2005). The ERA-40 re-analysis. *Quarterly Journal of the Royal Meteorological Society* 131, 2961–3012.
- van den Hurk, B., Best, M., Dirmeyer, P., Pitman, A., Polcher, J., and Santanello, J. (2011). Acceleration of land surface model development over a decade of GLASS. *Bulletin of the American Meteorological Society* 92, 1593–1600.
- Verseghy, D. L. (1991). CLASS—A Canadian land surface scheme for GCMs. I. Soil model. *International Journal of Climatology* 11, 111–133.
- Verseghy, D. L. (2011) CLASS—The Canadian land surface scheme (version 3.5). Technical Documentation (version 1). Environment Canada, Climate research division, Science and Technology branch.
- Verseghy, D. L., McFarlane, N. A., and Lazare, M. (1993). CLASS—A Canadian land surface scheme for GCMs, II. Vegetation model and coupled runs. *International Journal of Climatology* 13, 347–370.
- Vidale, P. L., Lüthi, D., Frei, C., Seneviratne, S. I., and Schär, C. (2003). Predictability and uncertainty in a regional climate model. *Journal of Geophysical Research : Atmospheres* 108, doi : 10.1029/2002JD002810.
- Webb, R. W., Rosenzweig, C. E., and Levine, E. R. (2000) Global soil texture and derived water-holding capacities. Oak Ridge National Laboratory Distributed Active Archive Center, Oak Ridge. <http://www.daac.ornl.gov>. doi :10.3334/ORNLDAAAC/548

- Xia, Y., Mitchell, K., Ek, M., Sheffield, J., Cosgrove, B., Wood, E., Luo, L., Alonge, C., Wei, H., Meng, J., and Livneh, B. (2012). Continental-scale water and energy flux analysis and validation for the North American Land Data Assimilation System project phase 2 (NLDAS-2) : 1. Intercomparison and application of model products. *Journal of Geophysical Research : Atmospheres* 117, D3, doi : 10.1029/2011JD016048.
- Xia, Y., Ford, T. W., Wu, Y., Quiring, S. M., and Ek, M. B. (2015). Automated Quality Control of in Situ Soil Moisture from the North American Soil Moisture Database Using NLDAS-2 Products. *Journal of Applied Meteorology and Climatology* 54, 1267–1282.
- Yeh, K. S., Côté, J., Gravel, S., Méthot, A., Patoine, A., Roch, M., and Staniforth, A. (2002). The CMC-MRB global environmental multiscale (GEM) model. Part III : Nonhydrostatic formulation. *Monthly Weather Review* 130, 339–356.
- Zadra, A., Caya, D., Côté, J., Dugas, B., Jones, C., Laprise, R., Winger, K., and Caron, L.-P. (2008). The next Canadian regional climate model. *Physics in Canada* 64, 75–83.
- Zhang, J., Wang, W. C., and Leung, L. R. (2008). Contribution of land-atmosphere coupling to summer climate variability over the contiguous United States. *Journal of Geophysical Research : Atmospheres* 113, D22, doi : 10.1029/2008JD010136.